

Supplementary Materials for

# Constrained C<sub>2</sub> adsorbate orientation enables CO-to-acetate electroreduction

Jian Jin<sup>1,2,18</sup>, Joshua Wicks<sup>3,18</sup>, QiuHong Min<sup>1,18</sup>, Jun Li<sup>4,18</sup>, Yongfeng Hu<sup>5</sup>, Jingyuan Ma<sup>6,7</sup>, Yu Wang<sup>6,7</sup>, Zheng Jiang<sup>6,7</sup>, Yi Xu<sup>8</sup>, Ruihu Lu<sup>1,9</sup>, Gangzheng Si<sup>1</sup>, Panagiotis Papangelakis<sup>8</sup>, Mohsen Shakouri<sup>10</sup>, Qunfeng Xiao<sup>10</sup>, Pengfei Ou<sup>3</sup>, Xue Wang<sup>3</sup>, Zhu Chen<sup>3</sup>, Wei Zhang<sup>11</sup>, Kesong Yu<sup>11</sup>, Jiayang Song<sup>1</sup>, Xiaohang Jiang<sup>1</sup>, Peng Qiu<sup>1</sup>, Yuanhao Lou<sup>1</sup>, Dan Wu<sup>1</sup>, Yu Mao<sup>9</sup>, Adnan Ozden<sup>8</sup>, Chundong Wang<sup>1</sup>, Bao Yu Xia<sup>12</sup>, Xiaobing Hu<sup>13,14</sup>, Vinayak P. Dravid<sup>13,14</sup>, Yun-Mui Yiu<sup>15</sup>, Tsun-Kong Sham<sup>15</sup>, Ziyun Wang<sup>9</sup>, David Sinton<sup>8</sup>, Liqiang Mai<sup>11\*</sup>, Edward H. Sargent<sup>3,16,17\*</sup>, Yuanjie Pang<sup>1\*</sup>

<sup>18</sup>These authors contributed equally to this work

\*Correspondence and requests for materials should be addressed to Edward H. Sargent, Yuanjie Pang, and Liqiang Mai ([ted.sargent@utoronto.ca](mailto:ted.sargent@utoronto.ca); [yuanjie\\_pang@hust.edu.cn](mailto:yuanjie_pang@hust.edu.cn); [mlq518@whut.edu.cn](mailto:mlq518@whut.edu.cn)).

## This PDF file includes:

Supplementary Text  
Figs. S1 to S43  
Tables S1 to S31

## Table of Contents

Techno-economic analysis .....	5
Supplementary Figures .....	13
Supplementary Fig. 1   Comparison of C-C coupling pathways .....	13
Supplementary Fig. 2   Comparison of the bifurcation of *(OH)C=COH → *C=C=O and *(OH)C=COH → *C=COH reaction pathways .....	14
Supplementary Fig. 3   Coverage-dependent phase diagram .....	15
Supplementary Fig. 4   SEM and size distribution of Cu/Ag-DA nanoparticles. ....	15
Supplementary Fig. 5   XPS spectrum of Ag and Cu atoms in Cu/Ag-DA catalysts. ....	16
Supplementary Fig. 6   TEM images of the as-synthesized catalysts before and after CORR. ....	16
Supplementary Fig. 7   Electrochemically active surface area (ECSA) measurements of Cu/Ag-DA catalysts. ....	17
Supplementary Fig. 8   SEM and EDX mapping images of Cu/Ag-DA catalysts. ....	18
Supplementary Fig. 9   SEM and EDX images of Cu/Ag-DA catalysts with an annealing temperature of 400 °C..	18
Supplementary Fig. 10   TEM characterization of Cu/Ag-DA nanoparticles. ....	19
Supplementary Fig. 11   EDS elemental analysis of the gold TEM grid. ....	20
Supplementary Fig. 12   XRD patterns of the Cu/Ag-DA catalysts before and after CORR. ....	20
Supplementary Fig. 13   XRD patterns of the Cu/M-DA (M = Ag, Au, and NiO) catalysts. ....	21
Supplementary Fig. 14   SEM and EDX mapping images of Cu/Au-DA catalysts. ....	21
Supplementary Fig. 15   XPS spectrum of Cu/Ni-DA catalysts. ....	22
Supplementary Fig. 16   Ex-situ XANES and first-derivative spectra. ....	22
Supplementary Fig. 17   Image of custom-built flow-cell for operando X-ray absorption spectroscopy. ....	23
Supplementary Fig. 18   Time-dependent operando Cu K-edge XAS of the Cu/Ag-DA catalyst .....	23
Supplementary Fig. 19   Operando EXAFS fitting. ....	24
Supplementary Fig. 20   In-situ Raman spectroscopy of Cu/Ag-DA and Ag materials. ....	25
Supplementary Fig. 21   Schematic of pressurized flow cell system. ....	27
Supplementary Fig. 22   NMR spectrum of liquid products from Cu/Ag-DA. ....	27
Supplementary Fig. 23   NMR spectrum of liquid products from Cu catalyst (Acetate, Ethanol, n-PrOH) ....	27
Supplementary Fig. 24   NMR spectrum of liquid products from Cu/Ag-DA using labeled C. ....	28
Supplementary Fig. 25   NMR spectrum of liquid products using Phenol as internal standard. ....	28
Supplementary Fig. 26   Gas chromatography analysis of the gas products of CORR. ....	29
Supplementary Fig. 27   Low-flow CO electroreduction using Cu/Ag-DA. ....	30

Supplementary Fig. 28   CO electroreduction in a pressurized flow cell with varying concentration of KOH electrolyte.....	30
Supplementary Fig. 29   XRD patterns of the Cu/Ag-DA catalysts with varying relative atomic ratios of Cu to Ag.....	31
Supplementary Fig. 30   SEM and EDX mapping images of Cu/Ag-DA catalysts prepared with ion implantation.....	31
Supplementary Fig. 31   CO electroreduction performance of Cu/Ag-DA prepared by copper ion implantation.....	32
Supplementary Fig. 32   XRD of the Cu/Ag-DA catalysts with annealing temperature of 400°C .....	32
Supplementary Fig. 33   CO electroreduction performance of Cu/Ag-DA annealed at different temperatures .....	33
Supplementary Fig. 34   CO electroreduction in a pressurized flow cell with Cu/Au-DA (a-c) and Cu/Ni-DA (d-f) catalyst.....	34
Supplementary Fig. 35   CO electroreduction in a pressurized flow cell using C and Ag control samples.....	35
Supplementary Fig. 36   Photograph of V1 MEA electrolyzer.....	35
Supplementary Fig. 37   Stability demonstration of Cu/Ag-DA in the V1 MEA cell over 50 hours.....	36
Supplementary Fig. 38   Image of liquid droplets on gas diffusion layer at the end of 50-hour experiment using the V1 pressurized MEA electrolyzer.....	36
Supplementary Fig. 39   Photograph of V2 MEA electrolyzer flow path .....	36
Supplementary Fig. 40   Stability demonstration of Cu/Ag-DA in the V2 MEA cell over >800 hours .....	37
Supplementary Note: Stability Experiments .....	37
Supplementary Fig. 41   Stability test of CORR to acetate with Cu/Ag-DA in a flow cell during ~12 hours of electrolysis .....	38
Supplementary Fig. 42   Process flow of TRL=3 complexity to electro-synthesize acetic acid from CO.....	38
Supplementary Fig. 43   Techno-economic Analysis of (a) CO-to-potassium acetate and (b) CO-to-acetic acid .....	39
Supplementary Tables .....	40
Supplementary Table 1   Inductive coupled plasma optical emission spectroscopy (ICP-OES) of the as-synthesized Cu/Ag-DA catalysts.....	40
Supplementary Table 2   Cu atomic ratio of catalysts studied in this work .....	40
Supplementary Table 3   Cu K-edge EXAFS fitting results of Cu/Ag-DA during CORR at different potentials (vs. RHE). ....	40
Supplementary Table 4   Vibrational frequencies of C <sub>2</sub> species on Ag <sub>35</sub> Cu <sub>1</sub> with 1 layer of H <sub>2</sub> O .....	41
Supplementary Table 5   Vibrational frequencies of C <sub>2</sub> species derived from <sup>12</sup> CO and <sup>13</sup> CO on Cu <sub>1</sub> Ag <sub>35</sub> model slab with 1 layer of H <sub>2</sub> O .....	42
Supplementary Table 6   Product FEs for Cu/Ag-DA under different applied potential in CORR.....	43
Supplementary Table 7   Comparison of prior CO <sub>2</sub> /CO-to-acetate reports.....	43
Supplementary Table 8   Raw Data for Fig. 4a.....	44
Supplementary Table 9   Raw Data for Fig. 4b .....	44

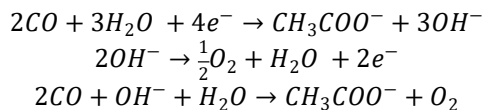
Supplementary Table 10   Raw Data for Fig. 4c .....	45
Supplementary Table 11   Raw Data for Fig. 4d .....	45
Supplementary Table 12   Raw Data for Fig. 4e .....	45
Supplementary Table 13   Raw Data for Supplementary Fig. 28 .....	47
Supplementary Table 14   Raw Data for Supplementary Fig. 31 .....	47
Supplementary Table 15   Raw Data for Supplementary Fig. 33 .....	47
Supplementary Table 16   Raw Data for Supplementary Fig. 34a .....	48
Supplementary Table 17   Raw Data for Supplementary Fig. 34b .....	48
Supplementary Table 18   Raw Data for Supplementary Fig. 34c .....	48
Supplementary Table 19   Raw Data for Supplementary Fig. 34d .....	48
Supplementary Table 20   Raw Data for Supplementary Fig. 34e .....	49
Supplementary Table 21   Raw Data for Supplementary Fig. 34f .....	49
Supplementary Table 22   Raw Data for Supplementary Fig. 37 .....	49
Supplementary Table 23   Raw Data for Supplementary Fig. 41 .....	49
Supplementary Table 24   Techno-economic model parameters .....	51
Supplementary Table 25   Raw Data for Supplementary Fig. 43 .....	52
Supplementary Table 26   Free energy corrections .....	52
Supplementary Table 27   Raw Data for Fig 1b, c .....	52
Supplementary Table 28   Raw Data for SI Fig 3 .....	52
Supplementary Table 29   Raw Data for Fig 1d. (Coverage Comparison) .....	53
Supplementary Table 30   Raw Data for Fig 1d. (Cluster Comparison) .....	53
Supplementary Table 31   DFT Models (Source data provided) .....	54
Supplementary Note: Adsorption of C <sub>2</sub> intermediates on low Cu concentration surfaces .....	61
References .....	62

## Techno-economic analysis

Our TEA model follows a general outline reported in a previous work<sup>1</sup> and all parameters are in **Supplementary Table 24**. Results are found in **Supplementary Table 25** and **Supplementary Fig. 43**.

We explored the costs to produce 100 tonnes of acetic acid per day (32,850 tonne per year, with a capacity factor of 0.9) over a 20-year factory life. We use an experimentally-derived MEA full-cell voltage of 2.3 V and an experimentally-derived total current density of 100 mA/cm<sup>2</sup> from our stability experiments to estimate a real voltage for a prospective industrial electrolyzer.

For the formation of acetate from CO, the chemical equation is:



Therefore, producing 1 mol of potassium acetate requires 2 mol of CO and 1 mol of KOH. However, the selectivity of CO-to-acetate is less than 100%, so more than 2 mol of CO is required.

### Electricity:

The production rate of Potassium Acetate in moles per second is:

$$KAcO \text{ production } \left( \frac{\text{mol}}{\text{s}} \right) = \frac{KAcO \text{ production } \left( \frac{\text{g}}{\text{day}} \right)}{M_{KAcO} \left( \frac{\text{g}}{\text{mol}} \right)} = \frac{100 \times \frac{10^6 \text{ g}}{\text{day}}}{\frac{98 \text{ g}}{\text{mol}} \times \frac{86400 \text{ s}}{\text{day}}} = 11.8 \frac{\text{mol}}{\text{s}}$$

Considering the loss of electrons due to FE below 100%, we find the current required to produce Potassium acetate at the target production rate:

$$I_{\text{total}} (A) = \frac{KAcO \text{ production } \left( \frac{\text{mol}}{\text{s}} \right) \times n \times F}{FE_{KAcO}} = \frac{11.8 \frac{\text{mol}}{\text{s}} \times 4 \times 96485 \frac{\text{sA}}{\text{mol}}}{91\%} = 5001 \text{ kA}$$

We multiply by the experimentally-derived MEA full-cell voltage (2.3 V) to get the power consumed:

$$\text{Power (kW)} = I_{\text{total}} \times V_{\text{cell}}(\text{V}) = 11503 \text{ kW}$$

We multiply the power consumption by 24 hr to get the energy consumed per 100 tonne of Potassium acetate produced. Multiplying the required energy by the electricity price (2 ¢/kWh) and dividing by the daily output of Potassium acetate, we then get the cost per tonne of Potassium acetate:

$$Cost_{\text{electricity}} \left( \frac{\$}{\text{tonne KAcO}} \right) = \frac{\text{Power} \times 24 \text{ hr} \times \text{price}_{\text{electricity}}}{KAcO \text{ production}} = \frac{15503 \text{ kW} \times 24 \text{ h} \times \frac{0.02\$}{\text{kWh}}}{100 \left( \frac{\text{tonne KAcO}}{\text{day}} \right)} = \frac{\$55.21}{\text{tonne KAcO}}$$

### Electrolyzer Capital Cost:

The reference electrolyzer cost is 450 \$/kW<sup>2</sup>, and the reference current density is 400 mA cm<sup>-2</sup>.

Multiplying by the unit price of the electrolyzer (450 \$/kW) and scaling by the current density (input current density is 100 mA cm<sup>-2</sup>), we get the total cost of the electrolyzer:

$$\begin{aligned}
Cost_{Total\ Electrolyzer} (\$) &= Power\ Consumed\ (kW) \times Cost_{Electrolyzer}\ (\$) \times \frac{base\ current\ density\left(\frac{mA}{cm^2}\right)}{input\ current\ density\left(\frac{mA}{cm^2}\right)} \\
&= 11503\ kW \times 450\ \frac{\$}{kW} \times \frac{400\left(\frac{mA}{cm^2}\right)}{100\left(\frac{mA}{cm^2}\right)} = \$20,704,974.26
\end{aligned}$$

The above is a one-time total cost of the electrolyzer, which must be converted to a cost per tonne of Potassium acetate. This technique of converting long-term investments into daily costs is used for all capital costs and uses a capital recovery factor (CRF) based on the discount rate  $i$  (7%) and the lifetime of the material (20 years).

$$CRF_{electrolyzer} = \frac{i(1+i)^{lifetime}}{(1+i)^{lifetime} - 1} = \frac{0.07(1.07)^{20}}{(1.07)^{20} - 1} = 0.094393$$

Next, we multiply the total electrolyzer capital cost by the CRF, and divide it by the number of days the plant operates and the daily Potassium acetate production. For all calculations, we assume that the factory has a capacity factor of 0.9.

$$\begin{aligned}
Cost_{electrolyzer} \left( \frac{\$}{tonne\ KAcO} \right) &= \frac{CRF_{electrolyzer} \times Cost_{electrolyzer}\ (\$)\left(\frac{mA}{cm^2}\right)}{Capacity\ factor \times 365\left(\frac{days}{year}\right) \times production\left(\frac{tonne\ KAcO}{day}\right)} \\
&= \frac{0.094393 \times \$20,704,974.26}{0.9 \times 365\left(\frac{days}{year}\right) \times 100\left(\frac{tonne\ KAcO}{day}\right)} = \frac{\$59.49}{tonne\ KAcO}
\end{aligned}$$

While most CO<sub>(2)</sub> electrolysis literature is reported at atmospheric pressure, this electrolyzer is pressurized to 10-20 atm. Some considerations for a large-scale system include reinforced pipes, reinforced reactor housings, and the need for high-pressure constant flow pumps. To account for additional potential costs for a system at pressure, we refer to the data in ref.<sup>3</sup> on biomass to fuel with Fischer-Tropsch. The total one-time pressure cost is assumed to 25% of the cost of the electrolyzer.

$$Cost_{pressure} \left( \frac{\$}{tonne\ KAcO} \right) = 0.25 \times Cost_{electrolyzer} \left( \frac{\$}{tonne\ KAcO} \right) = \frac{\$14.87}{tonne\ KAcO}$$

### **Catalyst and Membrane Costs:**

For catalyst and membrane costs, we assume 5% of the electrolyzer cost. We use the same procedure as described above to find the cost per tonne of Potassium acetate using a catalyst/membrane lifetime of 5 years:

$$\begin{aligned}
CRF_{C\&M} &= \frac{i(1+i)^{lifetime}}{(1+i)^{lifetime} - 1} = \frac{0.07(1.07)^5}{(1.07)^5 - 1} = 0.24389 \\
Cost_{C\&M} \left( \frac{\$}{tonne\ KAcO} \right) &= \frac{CRF_{C\&M} \times Cost_{Total\ Electrolyzer}\ (\$) \times 5\%}{Capacity\ factor \times 365\left(\frac{days}{year}\right) \times production\left(\frac{tonne\ KAcO}{day}\right)} \\
&= \frac{0.24389 \times \$20,704,974.26 \times 5\%}{0.9 \times 365\left(\frac{days}{year}\right) \times 100\left(\frac{tonne\ KAcO}{day}\right)} = \frac{\$7.69}{tonne\ KAcO}
\end{aligned}$$

## Cathode Gas Separation:

Gaseous side products ( $\text{H}_2$ ,  $\text{C}_2\text{H}_4$ ) are separated out of the CO outlet stream to enable the recirculation of unreacted CO. We calculate gaseous separation costs using estimates from a reference pressure-swing adsorption (PSA) system, provided in [Supplementary Table 24](#).

$$\begin{aligned} H_2 \text{ production rate } \left( \frac{\text{mol}}{\text{s}} \right) &= \frac{\text{Total Current} \times FE_{H_2}}{\# \text{ of electrons} * F} = \frac{5001202 \text{ A} \times 2\%}{2 e^- \times 96485 \frac{\text{C}}{\text{mol}}} = 0.52 \frac{\text{mol}}{\text{s}} \\ H_2 \text{ Flow Rate } \left( \frac{\text{m}^3}{\text{h}} \right) &= \frac{H_2 \text{ production rate} \times R \times T}{P} = \frac{0.52 \frac{\text{mol}}{\text{s}} \times 8.314 \frac{\text{J}}{\text{mol K}} \times 298 \text{ K}}{10 \text{ atm}} = 4.56 \frac{\text{m}^3}{\text{h}} \end{aligned}$$

The sum of gaseous side product flow rates and the flow rate of unreacted CO is used to estimate the gaseous separation cost:

$$\begin{aligned} \text{Gas Separation Operational Cost } \left( \frac{\$}{\text{tonne}} \right) &= \frac{\text{total flow rate} \times \text{reference PSA cost} \times \text{electricity price}}{\text{target output production}} \\ &= 10.84 \frac{\text{m}^3}{\text{h}} \times 24 \frac{\text{h}}{\text{day}} \times 0.25 \frac{\text{kWh}}{\text{m}^3} \times 0.02 \frac{\$}{\text{kWh}} \div 100 \frac{\text{tonne KAcO}}{\text{day}} = \frac{\$0.01}{\text{tonne KAcO}} \\ \text{Gas Separation Capital Cost } \left( \frac{\$}{\text{tonne}} \right) &= \frac{\text{reference PSA capital cost} \times (\frac{\text{total flow rate}}{\text{reference capacity}})^{\text{scaling factor}} \times \text{CRF}}{\text{Capacity factor} \times 365 \times \text{target output production}} \\ &= \frac{\$1989043 \times (\frac{10.84 \frac{\text{m}^3}{\text{h}}}{1000 \frac{\text{m}^3/\text{h}}{\text{day}}})^{0.7} \times 0.094}{0.9 \times 365 \frac{\text{day}}{\text{year}} \times 100 \frac{\text{tonne KAcO}}{\text{day}}} = \frac{\$0.24}{\text{tonne KAcO}} \end{aligned}$$

## Liquid Product Separation:

Distillation is a widely used liquid product separation method in  $\text{CO}_2\text{RR/CORR}^4$ . Recent literature has noted that azeotropic distillation is needed for the separation of acetic acid and water<sup>5</sup>. Here we fit the results of Aspen Plus Simulation from that work into an equation that depends on the concentration in the outlet stream ([Supplementary Table 24](#)). In [Supplementary Fig. 37](#), we obtain a product concentration of 1M after 50 hours and use this value here.

$$\begin{aligned} \text{Liquid Separation Operational Cost } \left( \frac{\$}{\text{tonne}} \right) &= -326.9 \times \ln(\text{product concentration}[M]) + 620.95 \\ &= \frac{\$620.95}{\text{tonne KAcO}} \\ \text{Liquid Separation Capital Cost } \left( \frac{\$}{\text{tonne}} \right) &= \frac{\text{reference distillation capital cost} \times (\frac{\text{total flow rate}}{\text{reference capacity}})^{\text{scaling factor}} \times \text{CRF}}{\text{Capacity factor} \times 365 \times \text{target output production}} \\ &= \frac{\$4162240.00 \times (\frac{66.55 \text{ L/min}}{1000 \text{ L/min}})^{0.7} \times 0.094}{0.9 \times 365 \frac{\text{day}}{\text{year}} \times 100 \frac{\text{tonne KAcO}}{\text{day}}} = \frac{\$1.80}{\text{tonne KAcO}} \end{aligned}$$

## Reactants:

### **Input CO:**

First, assuming there are no losses, we calculate the input CO required to produce 100 tonnes of potassium acetate.

$$CO_{\text{required}} \left( \frac{\text{tonne CO}}{\text{day}} \right) = \sum_i (\text{production rate} \left( \frac{\text{tonne}_i}{\text{day}} \right) \times \frac{M_{\text{CO}}}{M_i} \times \text{molar ratio} \left( \frac{CO}{i} \right))$$

Where  $i$  = acetate, ethylene, ethanol, n-propanol, and methane

$$\begin{aligned} CO_{\text{required}} \left( \frac{\text{tonne CO}}{\text{day}} \right) &= \left( \frac{100 \text{ tonne KAcO}}{\text{day}} \times \frac{28}{98} \times 2 \right) + \left( 0.79 \frac{\text{tonne C2H4}}{\text{day}} \times \frac{28}{28.05} \times 2 \right) + \left( 0.52 \frac{\text{tonne C2H5OH}}{\text{day}} \right. \\ &\quad \left. \times \frac{28}{46.07} \times 2 \right) = 59.3 \frac{\text{tonne CO}}{\text{day}} \end{aligned}$$

Now, we multiply this by a market price for CO (\$300/tonne)<sup>6</sup> and divide by the daily potassium acetate production. Prior literature for the cost to produce CO from a solid oxide electrolysis cell (SOEC) estimates 300-400 \$/tonne-CO, including electrolysis and separation<sup>7</sup>.

$$Cost_{\text{input CO}} \left( \frac{\$}{\text{tonne KAcO}} \right) = \frac{\$300}{\text{tonne CO}} \times 59.3 \frac{\text{tonne CO}}{\text{day}} \times \frac{1}{100 \text{ tonne KAcO}} = \frac{\$177.81}{\text{tonne KAcO}}$$

### Input KOH:

Here we use a KOH price of 790 USD/tonne<sup>8</sup>, as reported for North America in September 2021. Calculate the required amount of KOH with the same method above:

$$\begin{aligned} KOH_{\text{required}} \left( \frac{\text{tonne KOH}}{\text{day}} \right) &= \text{product output} \left( \frac{\text{tonne product}}{\text{day}} \right) \times \frac{M_{\text{KOH}}}{M_{\text{product}}} \times \text{molar ratio} \left( \frac{KOH}{\text{product}} \right) \\ KOH_{\text{required}} \left( \frac{\text{tonne KOH}}{\text{day}} \right) &= \frac{100 \text{ tonne KAcO}}{\text{day}} \times \frac{56.11}{98.15} \times 1 = 57.17 \frac{\text{tonne KOH}}{\text{day}} \end{aligned}$$

Now, multiplying by the KOH price (790 USD/ton) and dividing by our daily production of potassium acetate. The final cost of the input KOH is:

$$Cost_{\text{input KOH}} \left( \frac{\$}{\text{tonne KAcO}} \right) = 790 \frac{\$}{\text{tonne KOH}} \times 57.17 \frac{\text{tonne KOH}}{\text{day}} \times \frac{1}{100 \text{ tonne KAcO}} = \frac{\$451.62}{\text{tonne KAcO}}$$

### Input water:

Calculate the required amount of water with the same method above:

$$\begin{aligned} H_2O_{\text{required}} \left( \frac{\text{tonne H}_2O}{\text{day}} \right) &= \text{product output} \left( \frac{\text{tonne product}}{\text{day}} \right) \times \frac{M_{H_2O}}{M_{\text{product}}} \times \text{molar ratio} \left( \frac{H_2O}{\text{product}} \right) \\ H_2O_{\text{required}} \left( \frac{\text{tonne H}_2O}{\text{day}} \right) &= \frac{100 \text{ tonne KAcO}}{\text{day}} \times \frac{18}{98} \times 1 = 18.35 \frac{\text{tonne H}_2O}{\text{day}} \end{aligned}$$

Now, multiplying by the cost of water (\$5/tonne) and dividing by our daily production of potassium acetate. The final cost of the input water is:

$$Cost_{\text{input H}_2O} \left( \frac{\$}{\text{tonne KAcO}} \right) = 5 \frac{\$}{\text{tonne H}_2O} \times 21.0 \frac{\text{tonne H}_2O}{\text{day}} \times \frac{1}{100 \text{ tonne KAcO}} = \frac{\$0.92}{\text{tonne KAcO}}$$

### Total cost of inputs:

$$Cost_{\text{all inputs}} \left( \frac{\$}{\text{tonne KAcO}} \right) = Cost_{CO} + Cost_{KOH} + Cost_{water} = 177.81 + 451.62 + 0.92 = \frac{\$630.35}{\text{tonne KAcO}}$$

### Other operating costs:

To consider the additional operating costs associated with operating the factory (such as labor and maintenance), we have added an additional cost equal to 10% of the electricity cost:

$$Cost_{Other\ operation} \left( \frac{\$}{tonne\ KAcO} \right) = Cost_{electricity} \left( \frac{\$}{tonne\ KAcO} \right) \times 0.1 = \frac{\$5.52}{tonne\ KAcO}$$

### Electrolyte cost:

Our electrolyte is 5M KOH. By using a fixed volume ratio of 100 L of electrolyte per square meter of electrolyzer, we can find the total volume of electrolyte needed.

$$\begin{aligned} Volume_{electrolyte} (L) &= Surface\ area_{electrolyzer} (m^2) \times 100 \left( \frac{L}{m^2} \right) = \frac{Total_{current} (A)}{Current\ density \frac{mA}{cm^2} \times \left( \frac{100cm}{1m} \right)^2} \times 100 \left( \frac{L}{m^2} \right) \\ &= \frac{5001201 A}{0.1 \frac{A}{cm^2} \times \left( \frac{100cm}{1m} \right)^2} \times 100 \left( \frac{L}{m^2} \right) = 500120 L \\ Mass_{salt} (g) &= molarity_{salt} \left( \frac{mol}{L} \right) \times Volume_{electrolyte} (L) \times molecular\ weight \left( \frac{g}{mol} \right) = 5 \times 406602 \times 56 \\ &= 140\ 308\ 708\ g \\ Cost_{electrolyte} (\$) &= Mass_{salt} (tonne) \times price_{salt} \left( \frac{\$}{tonne} \right) + Volume_{water} (L) \times price_{water} \left( \frac{\$}{tonne} \right) \\ &= 140\ tonne \times 790 \frac{\$}{tonne} + 500120 L \times 5 \frac{\$}{tonne} = \$113,344.48 \end{aligned}$$

To get the cost per tonne of potassium acetate, we calculate the new CRF (1.07) by assuming an electrolyte lifetime of one year. Electrolyte costs per tonne of Potassium acetate:

$$\begin{aligned} Cost_{electrolyte} \left( \frac{\$}{tonne\ KAcO} \right) &= \frac{CRF_{electrolyzer} \times Cost_{electrolyte} (\$)}{Capacity\ factor \times 365 \left( \frac{days}{year} \right) \times production \left( \frac{tonne\ KAcO}{day} \right)} \\ &= \frac{1.07 \times \$113,344.48}{0.9 \times 365 \left( \frac{days}{year} \right) \times 100 \left( \frac{tonne\ KAcO}{day} \right)} = \frac{\$3.69}{tonne\ KAcO} \end{aligned}$$

### Total Operational Cost:

This is the combined total of electricity, electrolyte, cathode gas separation, cathode liquid separation, and other operating costs.

$$Cost_{Total\ Operational} \left( \frac{\$}{tonne\ KAcO} \right) = 55.21 + 3.69 + 0.01 + 620.95 + 5.52 = \frac{\$685.39}{tonne\ KAcO}$$

### Balance of Plant and Installation:

All capital costs are scaled to estimate the price of peripheral equipment around the electrolyzer and separation units. We assume a balance of plant (BoP) of 50% and a Lang factor of 1. To find our total capital costs, we sum the cost of electrolyzer, membrane & catalyst, and cathode separation capital.

$$\begin{aligned} Cost_{Total\ Capital} \left( \frac{\$}{tonne\ KAcO} \right) &= 59.49 + 7.69 + 14.87 + 0.24 + 1.80 = \frac{\$84.09}{tonne\ KAcO} \\ BOP \left( \frac{\$}{tonne\ KAcO} \right) &= BOP\ Factor \times Cost_{Total\ Capital} = 0.5 \times \frac{\$84.09}{tonne\ KAcO} = \frac{\$42.05}{tonne\ KAcO} \\ Cost_{Installation} \left( \frac{\$}{tonne\ KAcO} \right) &= Lang\ Factor \times Cost_{Total\ Capital} = 1 \times \frac{\$84.09}{tonne\ KAcO} = \frac{\$94.09}{tonne\ KAcO} \end{aligned}$$

### **Potassium Acetate Summary:**

By summing up all the above costs, we get the cost to produce one tonne of Potassium acetate in an electrolyzer:

$$\begin{aligned} Cost_{KAcO} &= Cost_{inputs} + Cost_{operational} + Cost_{Capital} + Cost_{installation} + BOP \\ &= 630.35 + 685.39 + 84.09 + 84.09 + 42.05 = \frac{\$1525.97}{\text{tonne KAcO}} \end{aligned}$$

### Prospective Upgrade to Acetic Acid:

Recent reports have shown an in-situ neutralization of potassium acetate to acetic acid<sup>9,10</sup>. Electrodialysis is another means to convert potassium acetate to acetic acid, and simultaneously recycle the K<sup>+</sup> ion in the form of KOH back to the beginning of the process flow. This is important because KOH is a significant input cost. A conservative energy estimate for electrodialysis is 5 kWh/kg-acid from ref<sup>9</sup>.

Recent literature has proposed using the cycling of HCl solution to protonate acetate and produce acetic acid<sup>5</sup>. This has an estimated energy cost of 1.58 kWh kg<sup>-1</sup> KOH and we use this value in our calculations herein.

Since the conversion to acetic acid recycles KOH back into the system, we subtract the cost for input KOH from the total, but keep the leveled electrolyte cost.

$$Cost_{KAcO \text{ less KOH}} = Cost_{KAcO} - Cost_{KOH} = \frac{\$1074.35}{\text{tonne } KAcO}$$

For every tonne of acetic acid produced, 1.64 tonnes of potassium acetate are needed.

$$\begin{aligned} Cost_{Acetic \text{ Acid}} &= \left( \frac{M_{KAcO}}{M_{acetic \text{ acid}}} \right) \times Cost_{KAcO \text{ less KOH}} + Cost_{electricity} \times Energy_{electrodialysis} \\ &= \frac{98 \frac{g-KAcO}{mol}}{60 \frac{g-acetic \text{ acid}}{mol}} \times 1074.35 \frac{\$}{\text{tonne } KAcO} + 0.02 \frac{\$}{kWh} \times 1580 \frac{kWh}{\text{tonne acetic acid}} = \frac{\$1772.84}{\text{tonne Acetic Acid}} \end{aligned}$$

### Energy Costs

We divide the energetic costs for a gate-to-gate CO<sub>2</sub>-to-acetate process between electrical energy, separation energy and the energy to produce CO from an SOEC.

For electrical energy:

$$E_{electrical}(\text{GJ/tonne}) = \frac{55.21 \frac{\$}{\text{tonne}}}{0.02 \frac{\$}{kWh}} \times 0.0036 \frac{\text{GJ}}{kWh} = 9.94 \text{ GJ/tonne}$$

For separation energy:

Assuming the operational separation cost of \$620.95/tonne-Potassium Acetate from the above calculation and the energy for this is provided by renewable electricity, we calculate:

$$E_{separation} \left( \frac{\text{GJ}}{\text{tonne}} \right) = \frac{\$620.95}{0.02 \frac{\$}{kWh}} \times 0.0036 \frac{\text{GJ}}{kWh} = 111.8 \frac{\text{GJ}}{\text{tonne}}$$

We use a solid oxide electrolysis cell (SOEC) to convert CO<sub>2</sub> to CO. The energy was estimated to be 13.49 GJ/ton-CO according to ref<sup>7</sup>.

$$E_{SOEC}(\text{GJ/tonne}) = CO_{\text{ required}}(\text{tonne}) \times 13.49 \frac{\text{GJ}}{\text{tonne}}$$

For the energy cost analysis of the direct CO<sub>2</sub>-to-Potassium Acetate pathway described in the main text, we use an anodic CO<sub>2</sub> crossover rate of 0.5 mol-CO<sub>2</sub>/mol-e<sup>-</sup> and an energy cost of 4 GJ/tonne-CO<sub>2</sub> for CO<sub>2</sub> removal<sup>11</sup>.

$$Anodic \text{ crossover} \left( \frac{\text{CO}_2}{\text{KAcO}} \right) = \frac{0.5 \frac{\text{mol CO}_2}{\text{mol e}^-}}{96485 \frac{\text{C}}{\text{mol e}^-}} \times \text{Current}[A] \times 44.1 \frac{\text{g}}{\text{mol}} \times \frac{1 \text{ tonne}}{10^6 \text{ g}} \times \frac{3600 \text{ s} \times 24 \text{ h}}{1 \text{ day}} \div 100 \frac{\text{tonne}}{\text{day}}$$

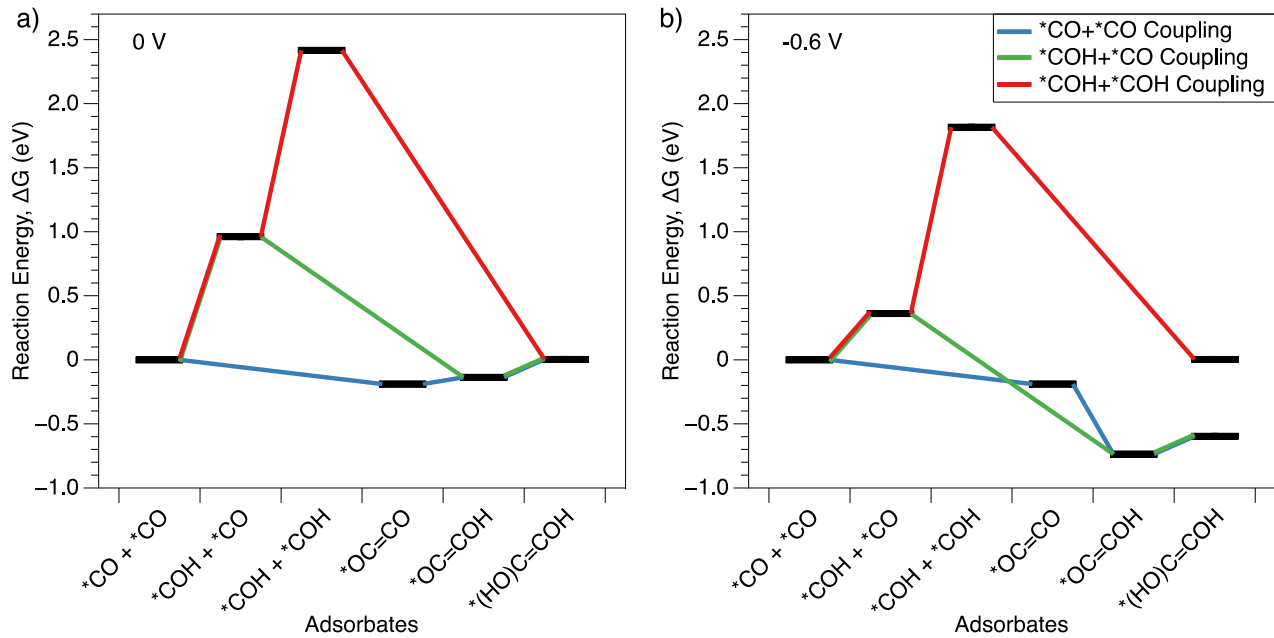
$$E_{\text{separation}} \left( \frac{\text{GJ}}{\text{tonne}} \right) = \left( \frac{\text{Cost}_{\text{separation}}}{0.02 \frac{\$}{\text{kWh}}} \times 0.0036 \frac{\text{GJ}}{\text{kWh}} \right) + \left( \text{Anodic Crossover} \left( \frac{\text{CO}_2}{\text{KAcO}} \right) \times \frac{4 \text{ GJ}}{\text{tonne CO}_2} \right)$$

Therefore, the total energy for production of one tonne of acetate (derived from CO<sub>2</sub>) can be expressed as follows:

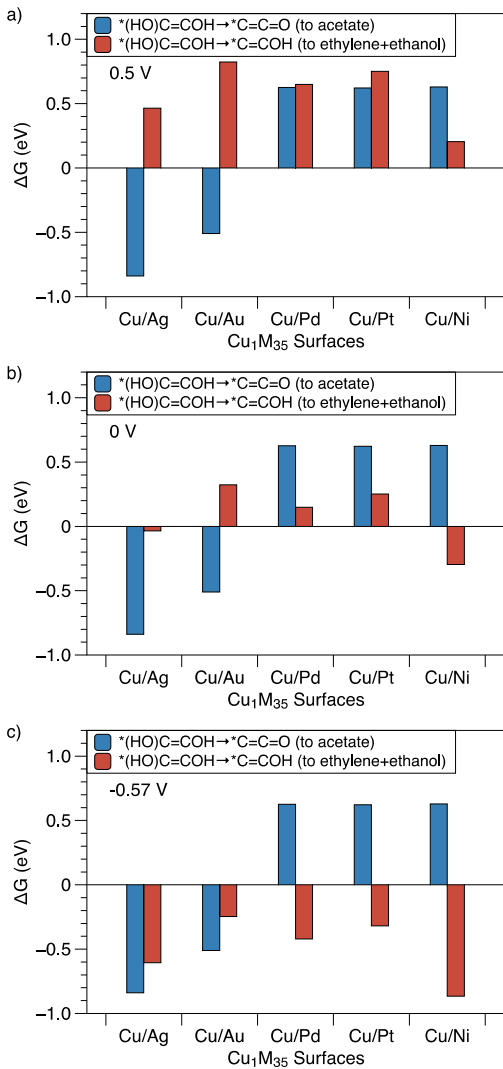
$$E_{\text{total}} \left( \frac{\text{GJ}}{\text{tonne}} \right) = E_{\text{electrical}} \left( \frac{\text{GJ}}{\text{tonne}} \right) + E_{\text{separation}} \left( \frac{\text{GJ}}{\text{tonne}} \right) + E_{\text{SOEC}} \left( \frac{\text{GJ}}{\text{tonne}} \right)$$

Although not reported in the reference CO<sub>2</sub>-to-Acetate pathway<sup>12</sup>, the same 0.33 M concentration was used for comparison with the reference CO-to-acetate pathway<sup>13</sup>.

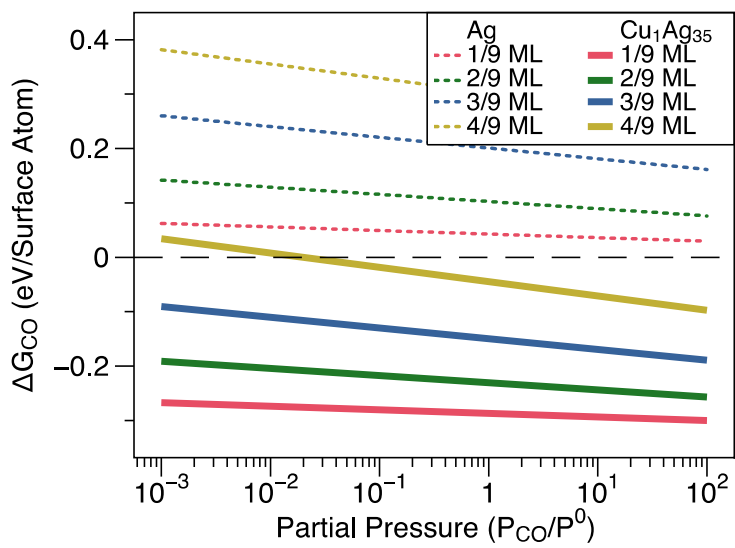
## Supplementary Figures



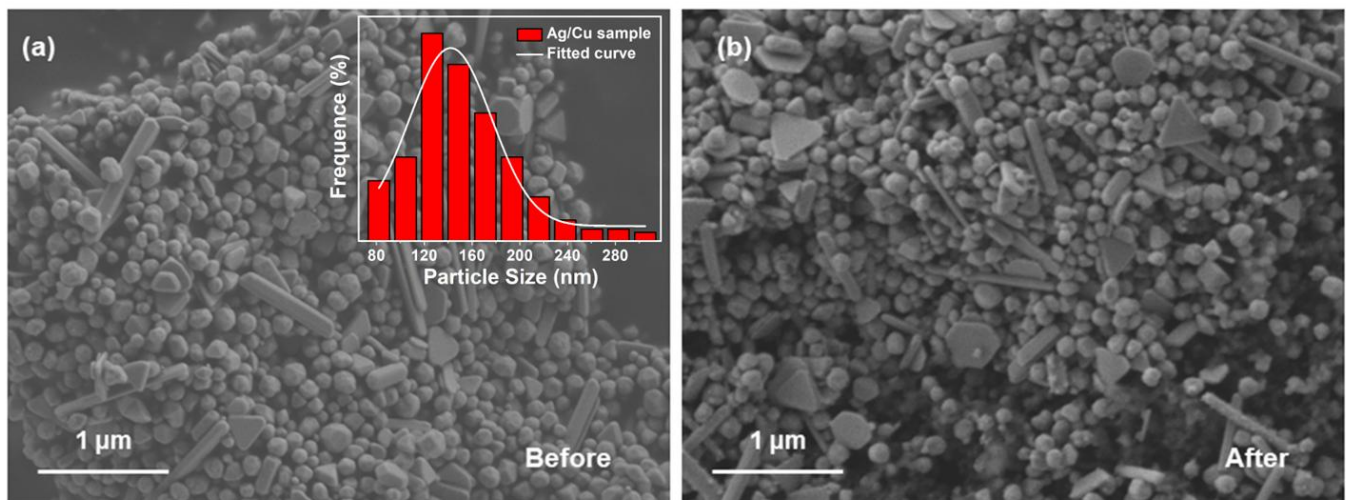
**Supplementary Fig. 1 |** Comparison of C-C coupling pathways from \*CO to \*(HO)C=COH on a Cu<sub>1</sub>Ag<sub>35</sub>(111) surface at a) 0 V and b) -0.6 V.



**Supplementary Fig. 2 |** Comparison of the bifurcation of  $^{*}(\text{OH})\text{C=COH} \rightarrow ^{*}\text{C=C=O}$  and  $^{*}(\text{OH})\text{C=COH} \rightarrow ^{*}\text{C=COH}$  reaction pathways as an indicator for acetate selectivity across a series of Cu/M-DAs (modeled as  $\text{Cu}_1\text{M}_{35}$ , M = Ag, Au, Pd, Pt, Ni) surfaces at a) 0.5 V, b) 0 V, and c) -0.57 V. 0.5 V is the thermodynamic voltage for CO-to-acetate electro-conversion. 0 V is the potential used in the Figure 1b of the main text and is repeated here for comparison. -0.57 V is the applied potential later shown in the manuscript to be optimal for acetate selectivity (91% FE). Since the  $^{*}\text{C=COH}$  pathway includes an explicit electron transfer and the  $^{*}\text{CCO}$  pathway does not, it is important to assess the relative difference between them at multiple potentials. We note that the  $^{*}(\text{OH})\text{C=COH} \rightarrow ^{*}\text{C=CO} + \text{H}_2\text{O}$  reaction step is not entirely independent of potential because it is still subject to field effects induced by the electric potential. These effects are captured using the charged water monolayer in the model. The breakeven point at which the relative difference between  $^{*}\text{C=C=O}$  and  $^{*}\text{C=COH}$  pathways is 0 occurs at -0.75 V. This voltage is more negative than the voltages where the peak selectivity to acetate is observed (91% FE at -0.57 V and 90% FE at -0.68 V). This agreement between theory and experiment suggests that for all experimentally-relevant applied potentials, the  $^{*}\text{CCO}$  pathway remains favored over the  $^{*}\text{C=COH}$  pathway. For experimentally applied voltages even more negative than -0.75 V, we do observe a decline in acetate FE; although this can also be attributed to other confounding factors, such as competition with HER at highly negative potentials and mass transport limitations at high rates.

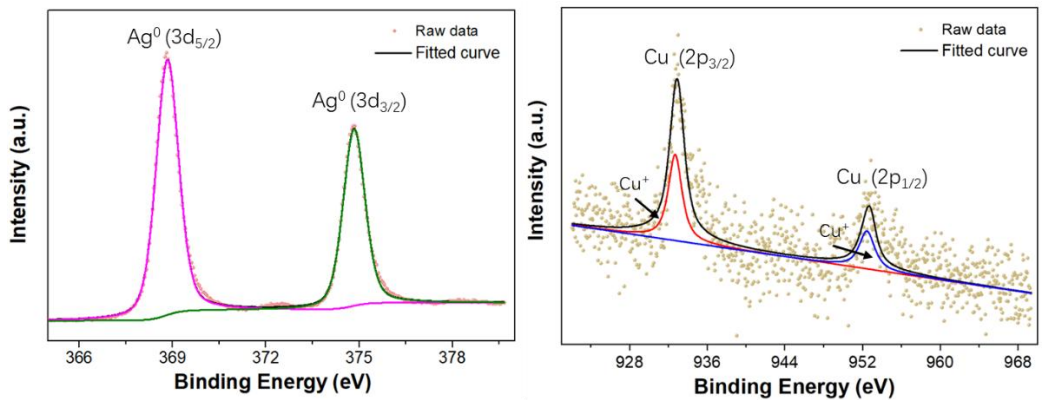


**Supplementary Fig. 3 |** Coverage-dependent phase diagram of  ${}^*\text{CO}$  adsorbed on Ag(111) and  $\text{Cu}_1\text{Ag}_{35}(111)$  surfaces.

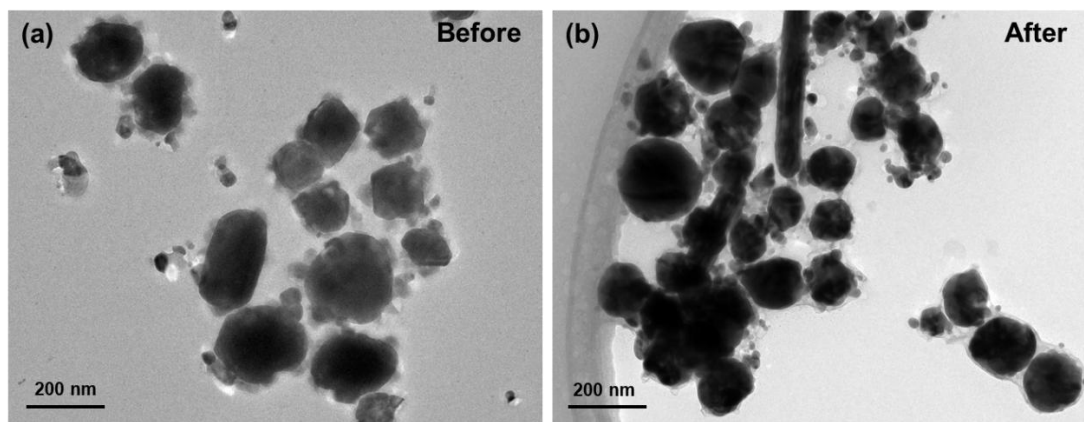


**Supplementary Fig. 4 | SEM and size distribution of Cu/Ag-DA nanoparticles.**

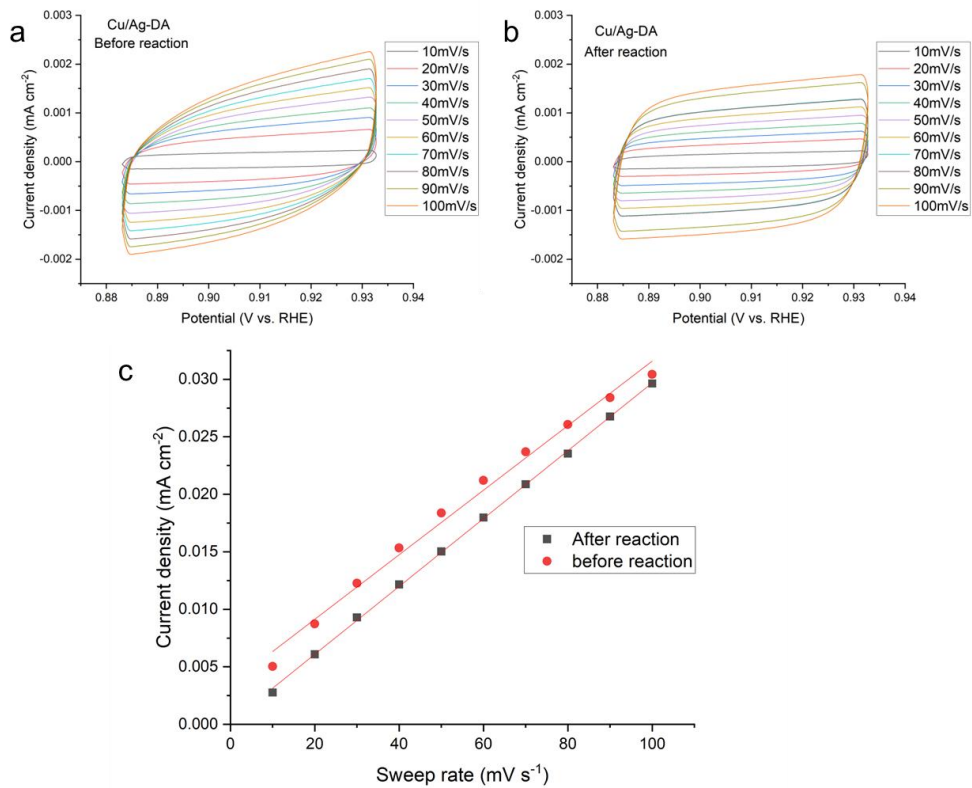
(a) Before and (b) after CORR.



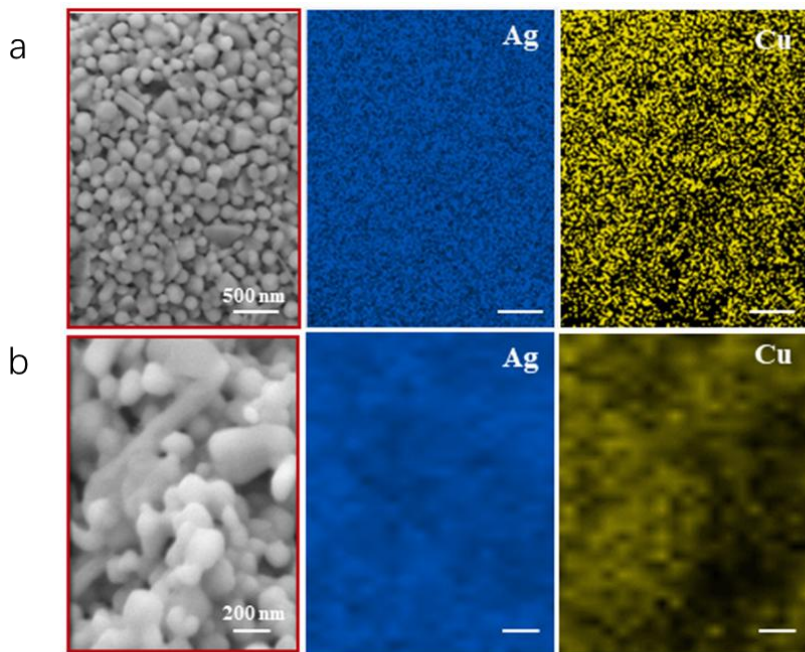
**Supplementary Fig. 5 | XPS spectrum of Ag and Cu atoms in Cu/Ag-DA catalysts.**



**Supplementary Fig. 6 | TEM images of the as-synthesized catalysts before and after CORR.**  
 (a) Before and (b) after CORR.

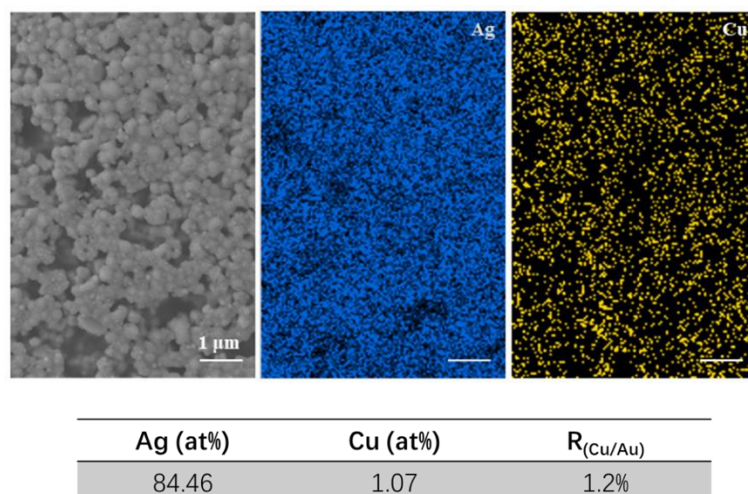


**Supplementary Fig. 7 | Electrochemically active surface area (ECSA) measurements of Cu/Ag-DA catalysts.** (a) Cyclic voltammetry profiles obtained from Cu/Ag-DA catalyst before and (b) after reaction at sweep rates of 10, 20, 30, 40, 50, 60, 70, 80, 90, and 100  $\text{mV}\cdot\text{s}^{-1}$ . (c) Double layer capacitance comparison for Cu/Ag-DA catalysts (before and after reaction).

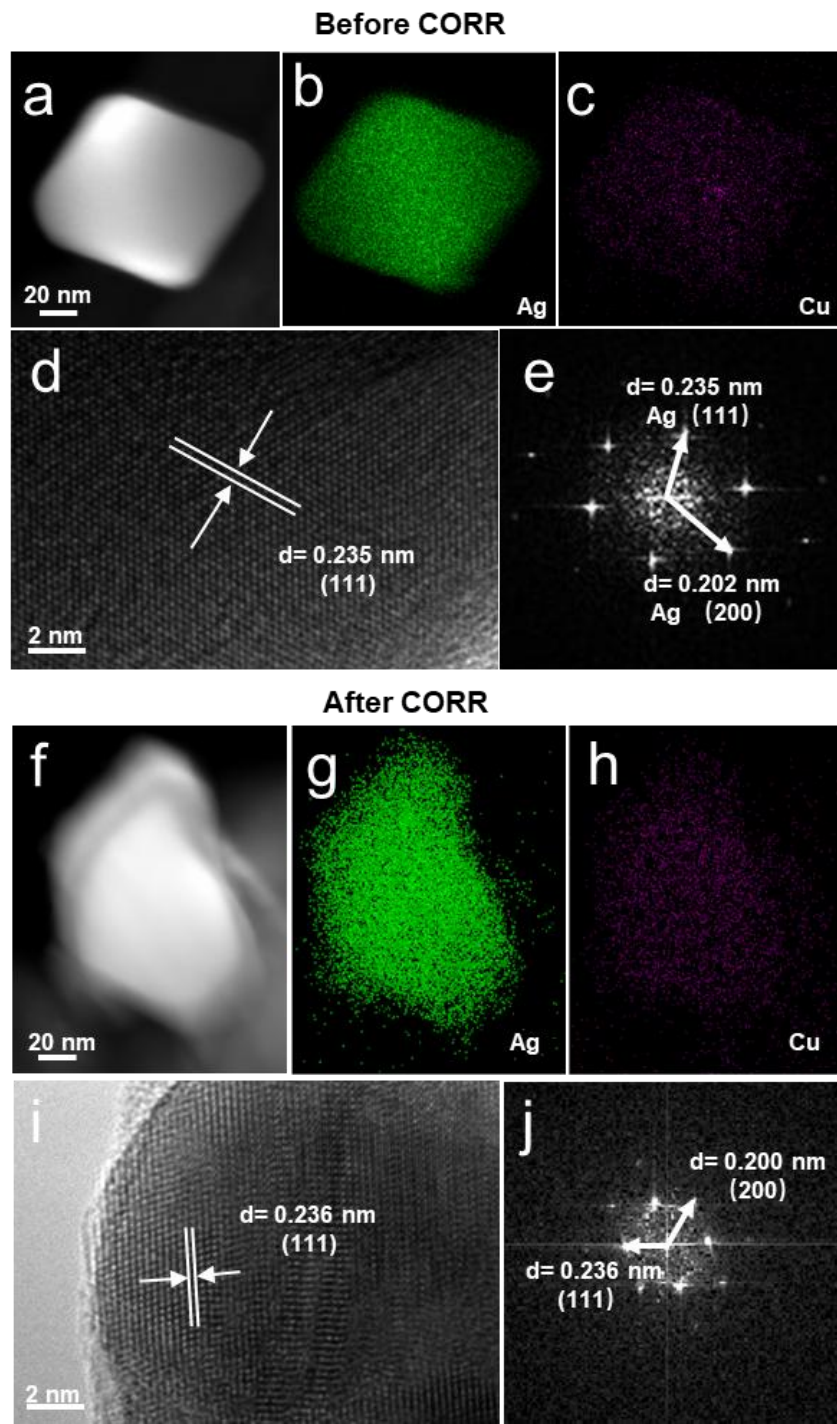


	Ag (at%)	O (at%)	Cu (at%)	$R_{(Cu/Ag)}$
a	92.18	7.13	0.1	0.1%
b	82.99	15.89	0.56	0.7%

**Supplementary Fig. 8 | SEM and EDX mapping images of Cu/Ag-DA catalysts.**

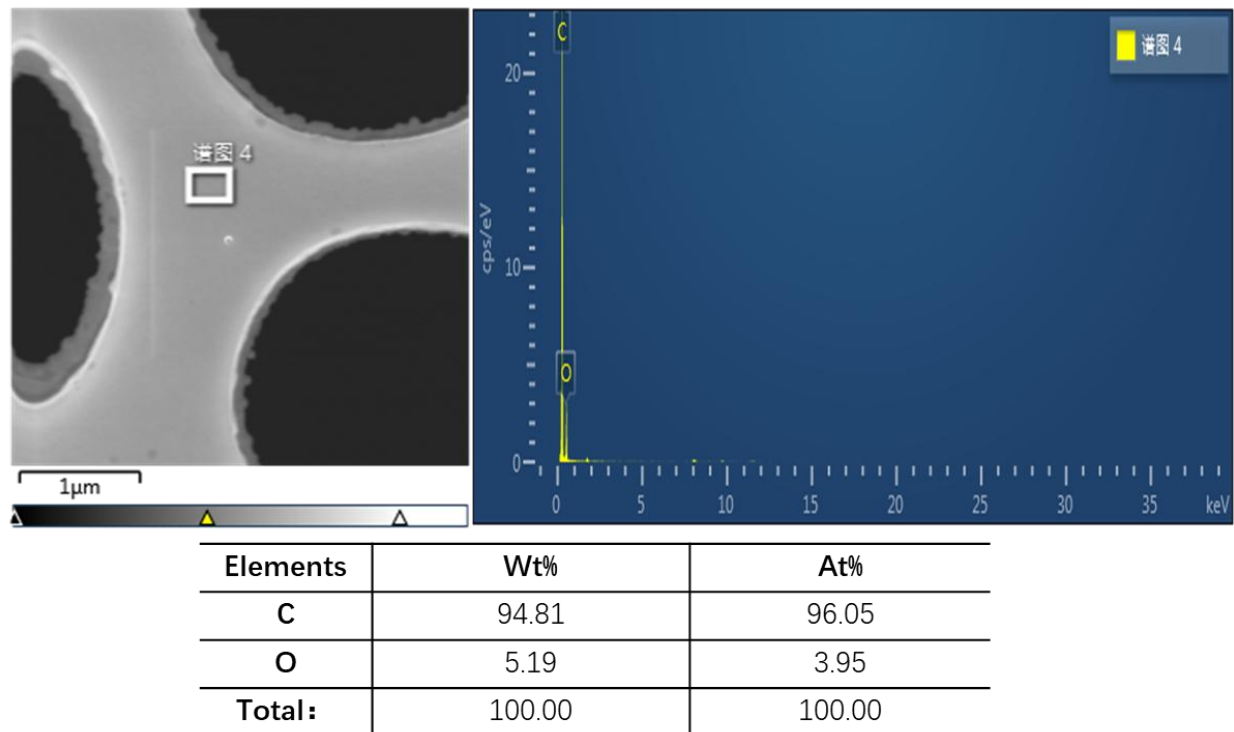


**Supplementary Fig. 9 | SEM and EDX images of Cu/Ag-DA catalysts with an annealing temperature of 400 °C.**

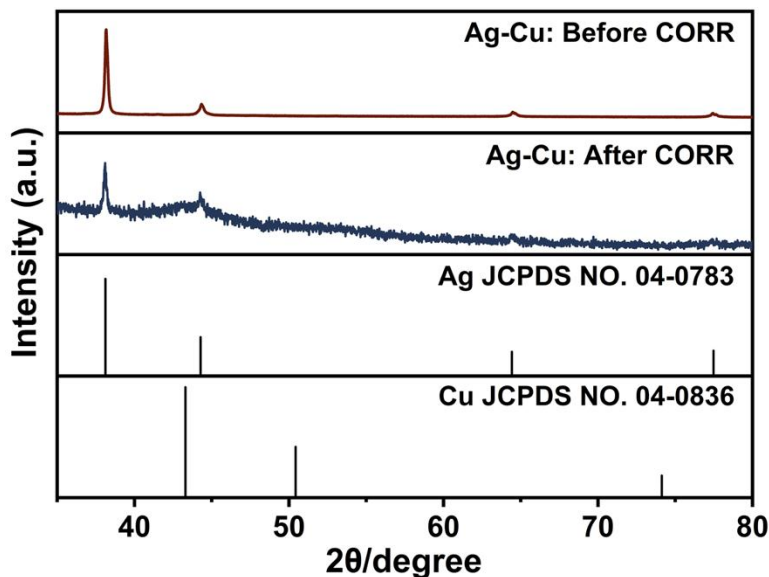


**Supplementary Fig. 10 | TEM characterization of Cu/Ag-DA nanoparticles.**

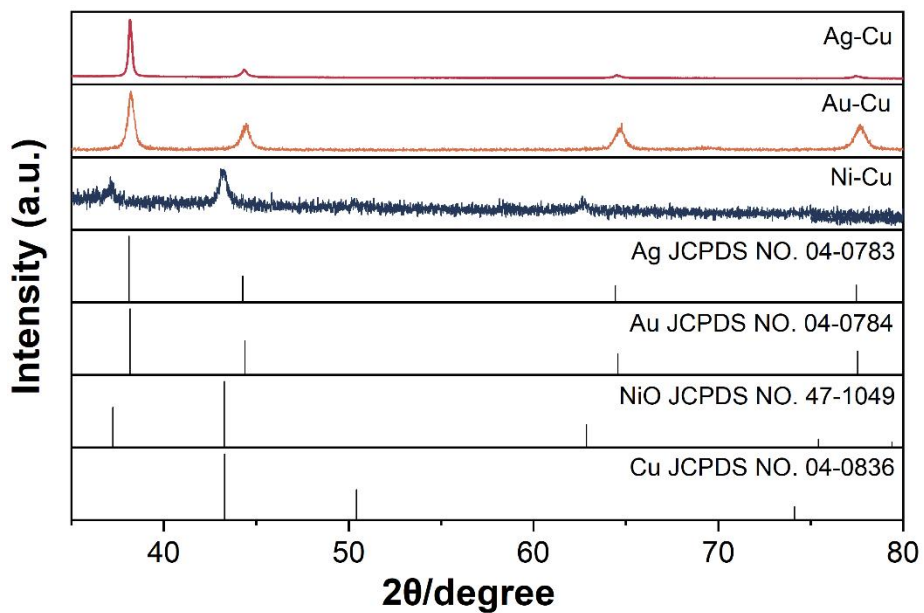
(a) TEM images of the as-synthesized catalysts before CORR. (b-e) EDX and HRTEM images of a single Cu/Ag-DA nanoparticle. (f) TEM images of the as-synthesized catalysts after CORR. (g-j) EDX and HRTEM images of a single Cu/Ag-DA nanoparticle after CORR.



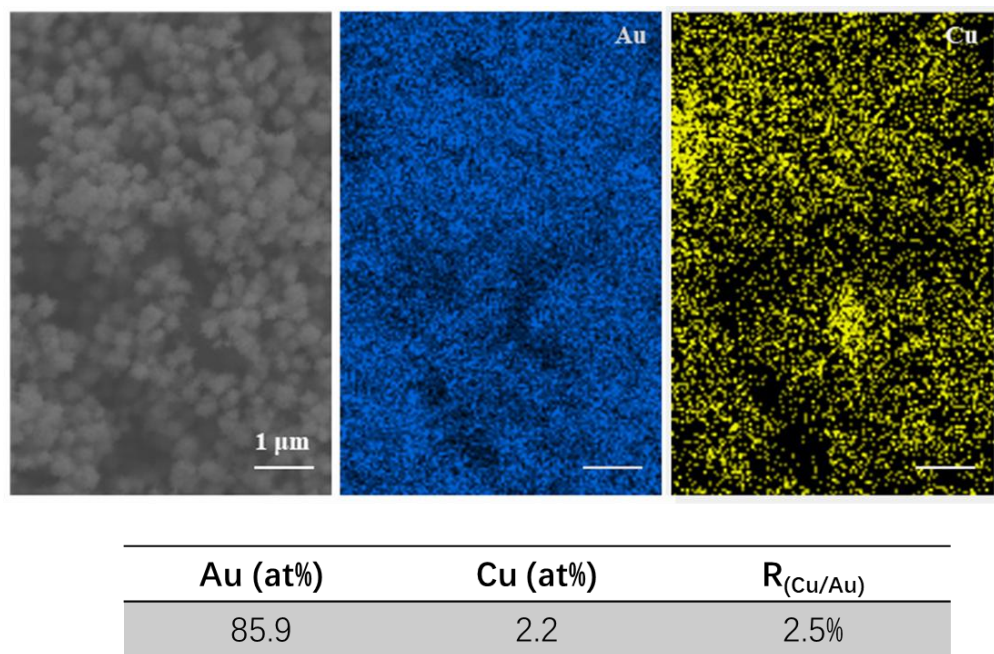
Supplementary Fig. 11 | EDS elemental analysis of the gold TEM grid.



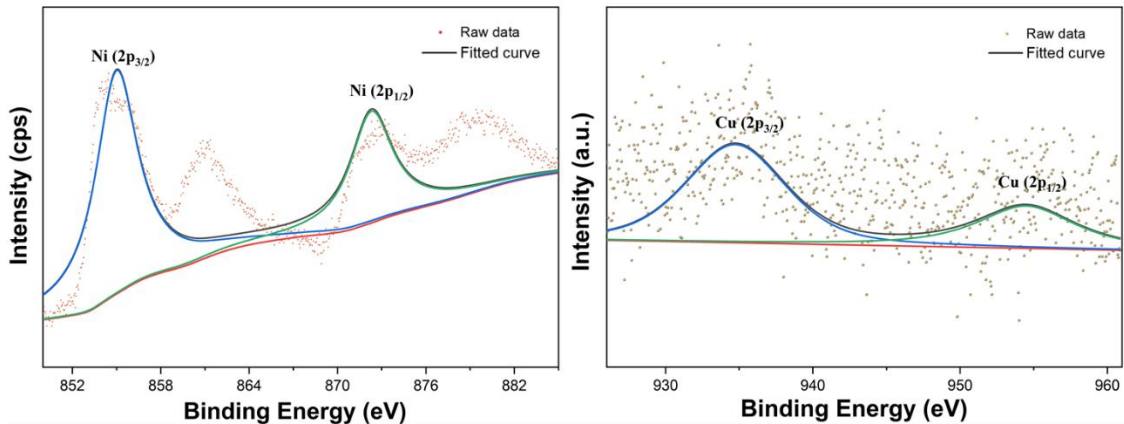
Supplementary Fig. 12 | XRD patterns of the Cu/Ag-DA catalysts before and after CORR.



**Supplementary Fig. 13 | XRD patterns of the Cu/M-DA (M = Ag, Au, and NiO) catalysts.**

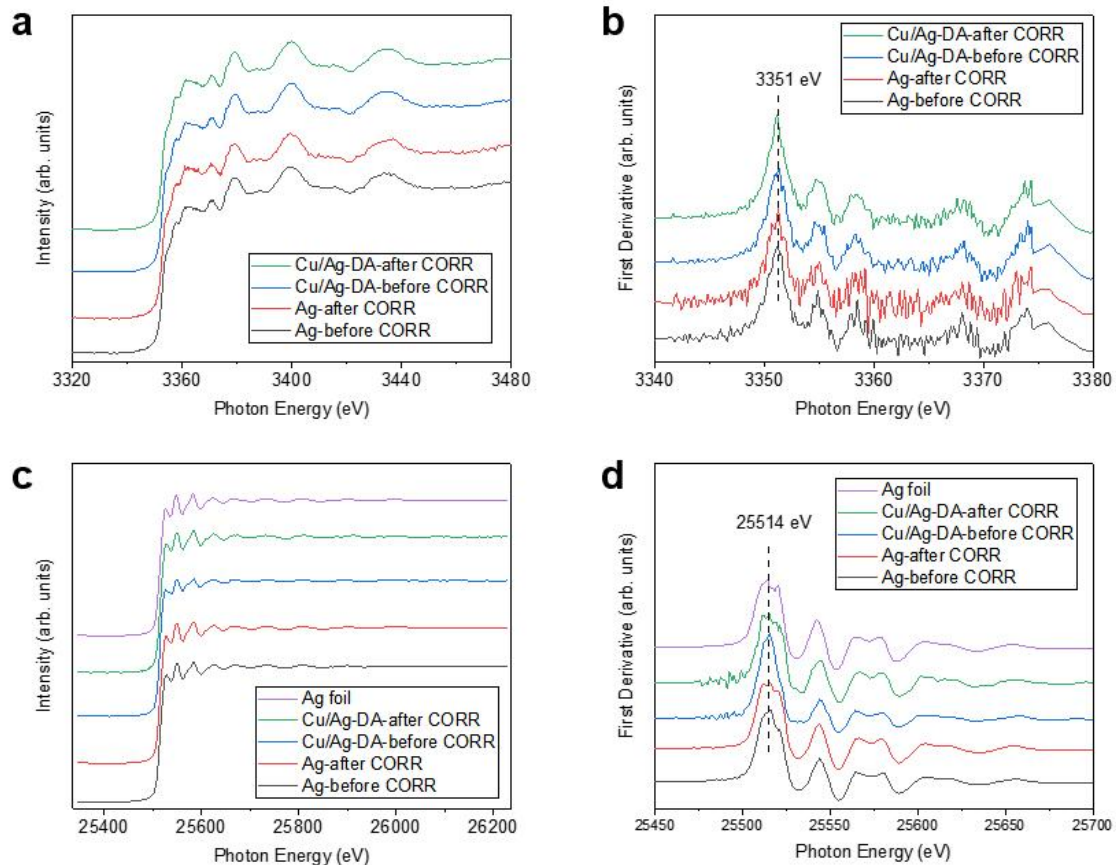


**Supplementary Fig. 14 | SEM and EDX mapping images of Cu/Au-DA catalysts.**

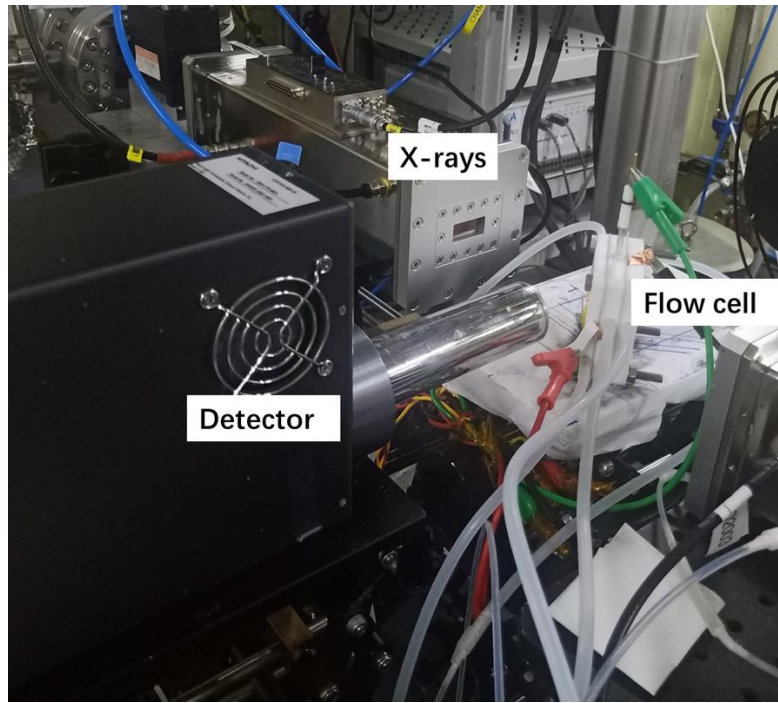


Ni	Cu	$R_{(Cu/Ni)}$
11.7	0.3	2.5%

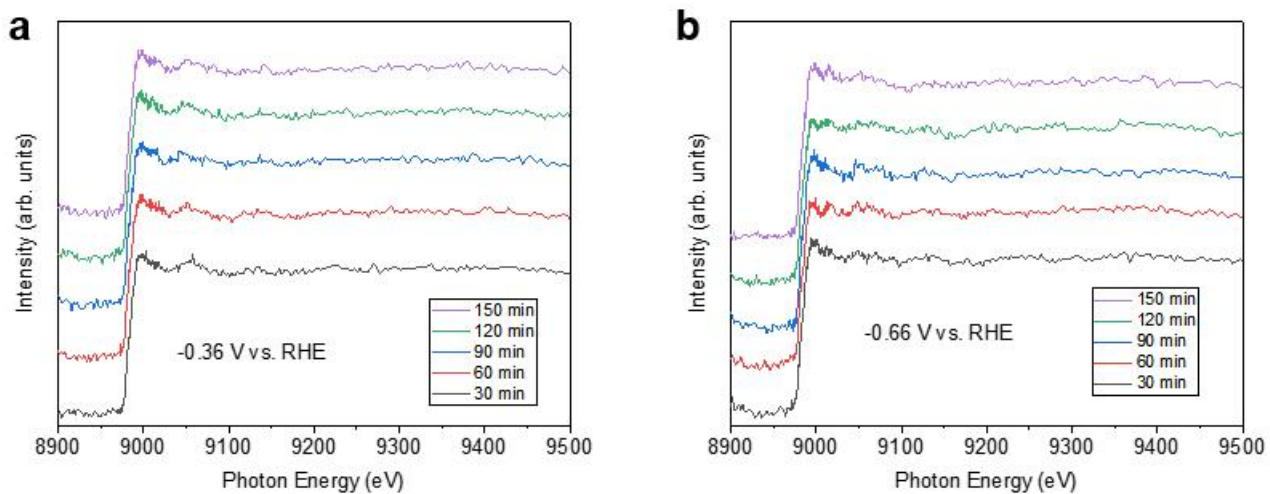
Supplementary Fig. 15 | XPS spectrum of Cu/Ni-DA catalysts.



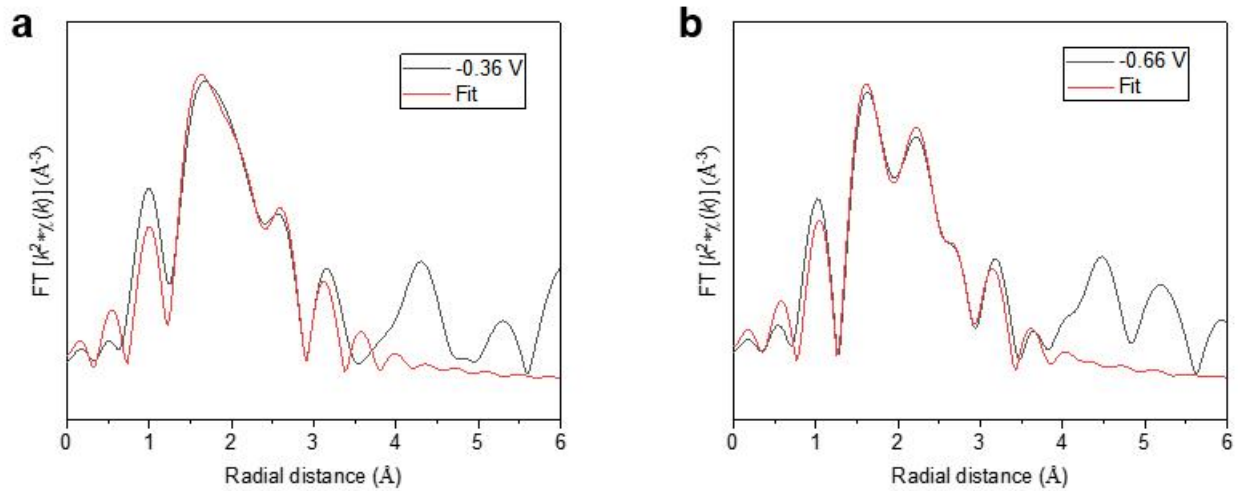
Supplementary Fig. 16 | Ex-situ XANES and first-derivative spectra. (a) Ex-situ Ag L<sub>3</sub>-edge XANES and (b) related first derivative spectra of the Cu/Ag-DA catalyst and the bare Ag catalyst before and after CORR. (c) Ex-situ Ag K-edge XANES and (d) related first derivative spectra of Cu/Ag-DA and bare Ag before and after CORR.



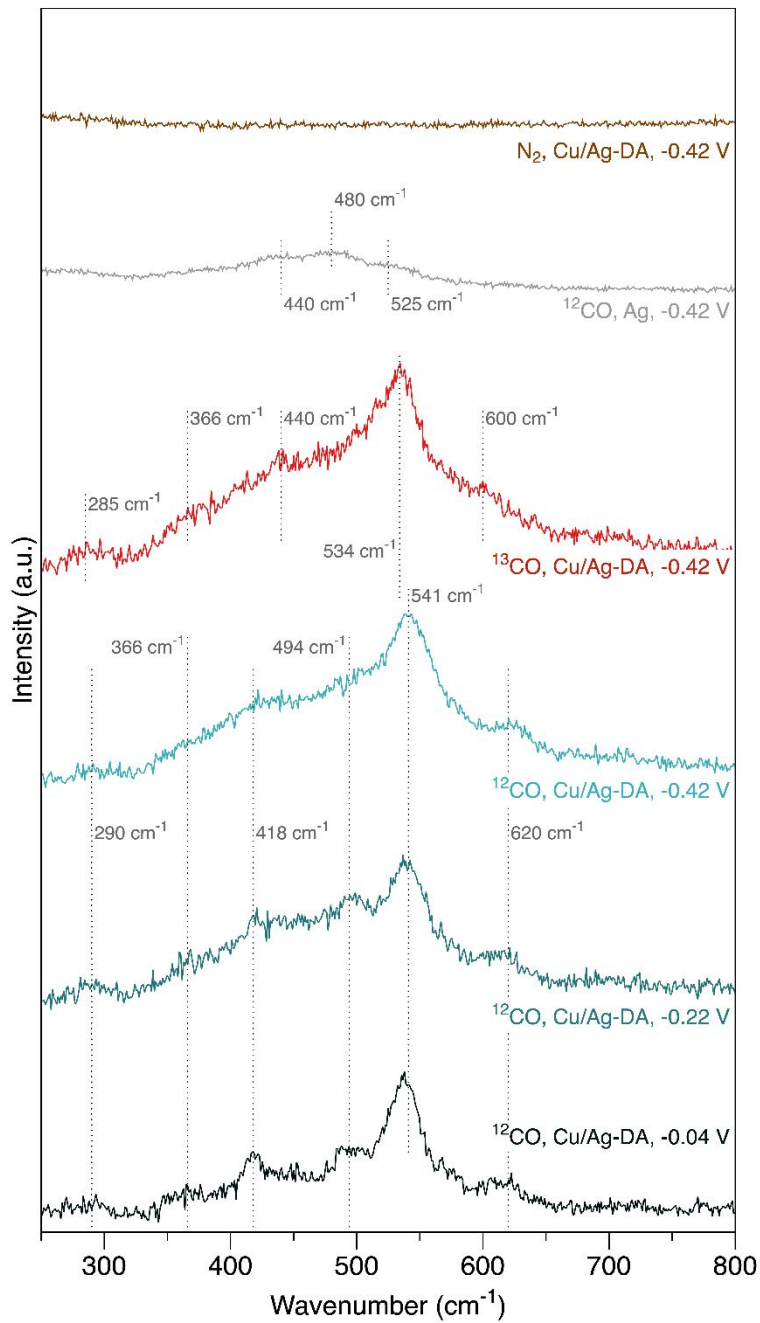
**Supplementary Fig. 17 | Image of custom-built flow-cell for operando X-ray absorption spectroscopy.**



**Supplementary Fig. 18 | Time-dependent operando Cu K-edge XAS of the Cu/Ag-DA catalyst at (a) -0.36 V and (b) -0.66 V.**



**Supplementary Fig. 19 | Operando EXAFS fitting.** Cu K-edge EXAFS fitting results of the Cu/Ag-DA catalyst during CORR at (a) -0.36 V and (b) -0.66 V.



**Supplementary Fig. 20 | In-situ Raman spectroscopy of Cu/Ag-DA and Ag materials.**

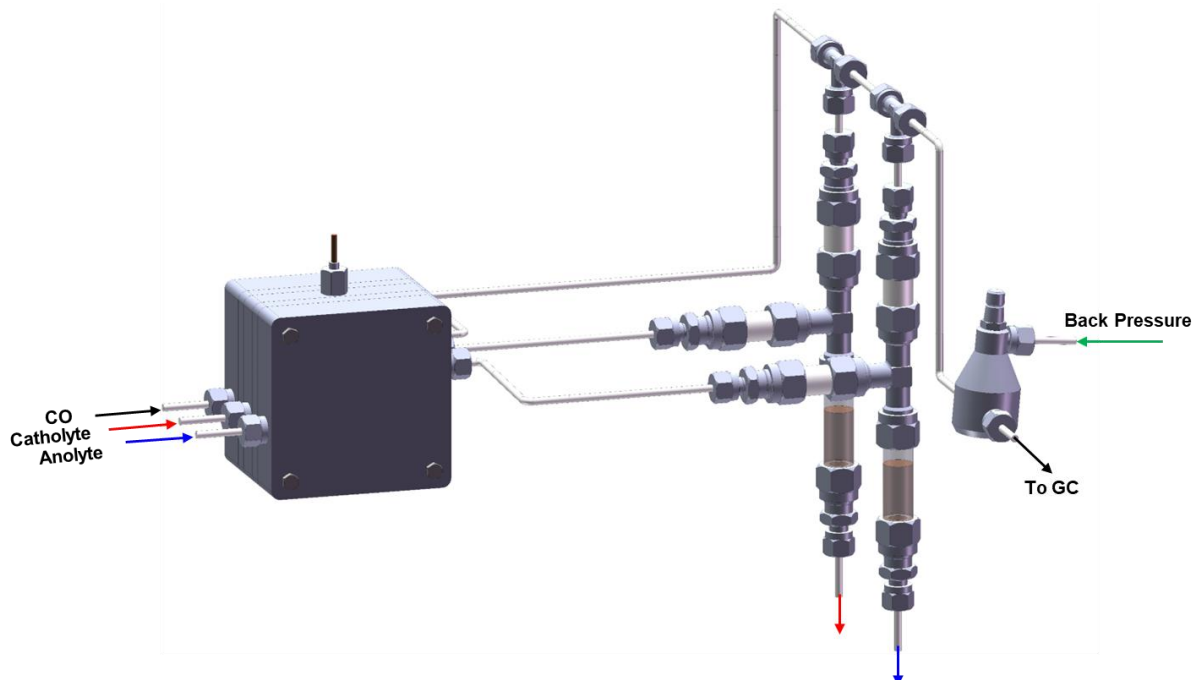
Spectroscopy data between 250 – 800 cm<sup>-1</sup> collected after ~3 min of electrolysis. Applied potentials in plot are vs. RHE.

Peaks at ~290, ~541 and ~620 cm<sup>-1</sup> shift to ~285, ~534 and ~600 cm<sup>-1</sup> when using labelled  $^{13}\text{CO}$  gas. These peaks are not present when CO is substituted for an inert gas ( $\text{N}_2$ ).  $^{13}\text{CO}$  and  $\text{N}_2$  controls indicate that these correspond to carbon-containing species. Other shifts among peaks in the 320–500 cm<sup>-1</sup> region are not easily assessed due to the broad nature of this region. We associate the small peaks from Cu/Ag-DA materials at 285–290 cm<sup>-1</sup> and 366 cm<sup>-1</sup> with Cu–CO frustrated rotation and Cu–CO stretching vibrations, respectively<sup>14–17</sup>. A composite triplet of peaks (broad region of 360–540

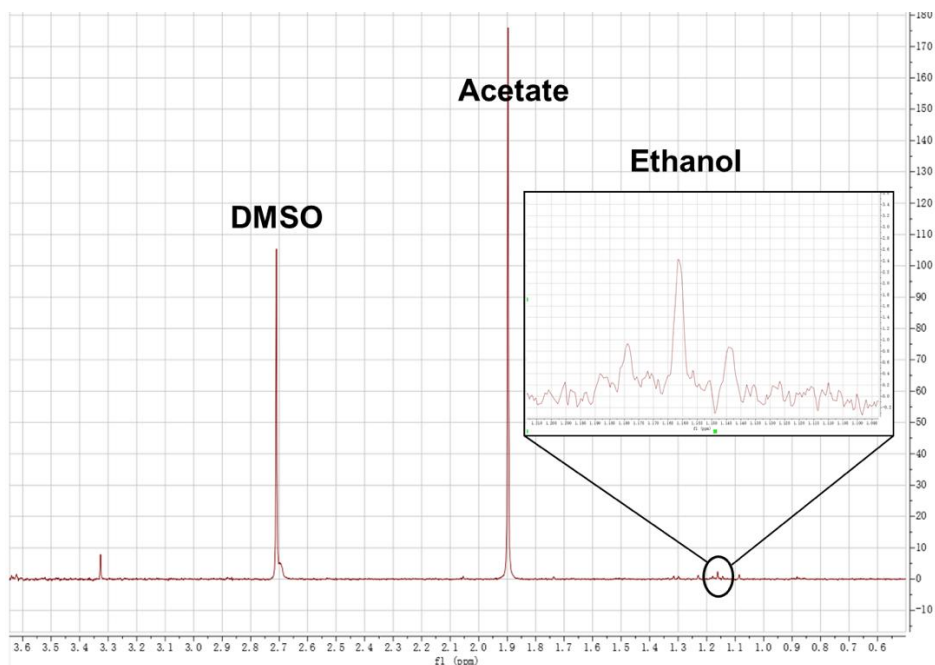
$\text{cm}^{-1}$ ) observed from the pure Ag sample is likely to be adsorbed  $^*\text{CO}$  on Ag<sup>14,15,17</sup>. Similarly, peaks at 418, 440, and 494  $\text{cm}^{-1}$  from Cu/Ag-DA samples are therefore attributed to  $^*\text{CO}$  on Ag. Peaks at 620  $\text{cm}^{-1}$  may be attributed to the out-of-plane rocking mode of ( $\text{COO}^-$ ) from locally-produced acetate. The in-plane rocking mode of ( $\text{COO}^-$ ) from locally-produced acetate is expected to be at 470  $\text{cm}^{-1}$  (not visible due to the overlap of peaks in this region)<sup>18</sup>. Contribution to the peak shoulder at  $\sim 595$   $\text{cm}^{-1}$  may also be related to the Cu-O<sub>ad</sub> stretching mode (570–630  $\text{cm}^{-1}$ )<sup>19</sup>.

The strongest peak at 541  $\text{cm}^{-1}$  is close to prior reports of Ag-CO vibrations which typically show a peak at 523–530  $\text{cm}^{-1}$ , but comparison to the pure Ag sample suggests this peak is related to another adsorbate. Calculated vibrational frequencies (Supplementary Tables 6 and 7) for a variety of potential adsorbates indicate that  $^*\text{C}=\text{C}=\text{O}$  or  $^*(\text{OH})\text{C}=\text{COH}$  adsorbates may correspond to this peak. Prior literature has hypothesized  $^*\text{C}=\text{C}=\text{O}$  and  $^*(\text{OH})\text{C}=\text{COH}$  to be potentially long-lived species on Cu<sup>20</sup>.

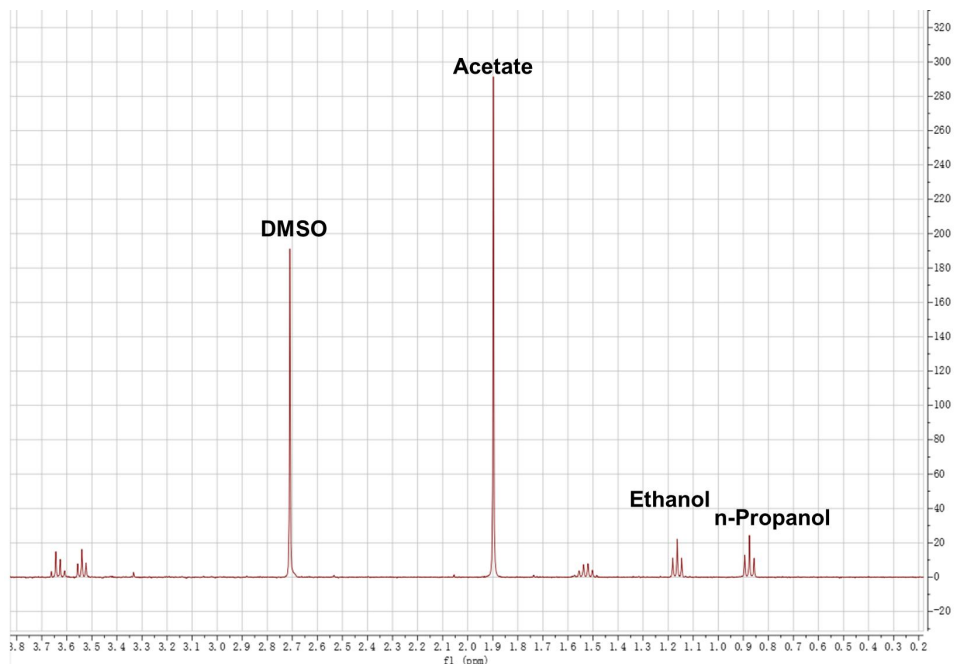
Broadening of all spectra between 200 and 750  $\text{cm}^{-1}$  may be related to the potential- and OH<sup>-</sup>-dependent libration of water on Ag and Ag-based materials<sup>21</sup>. Residual copper oxide clusters may also contribute to broadening in this region with reported peaks at 415, 527, and 623  $\text{cm}^{-1}$ <sup>15</sup>, but a Stark shift with more negative potential suggests that the 620  $\text{cm}^{-1}$  peak is related to an adsorbate and not a significant presence of copper oxide.



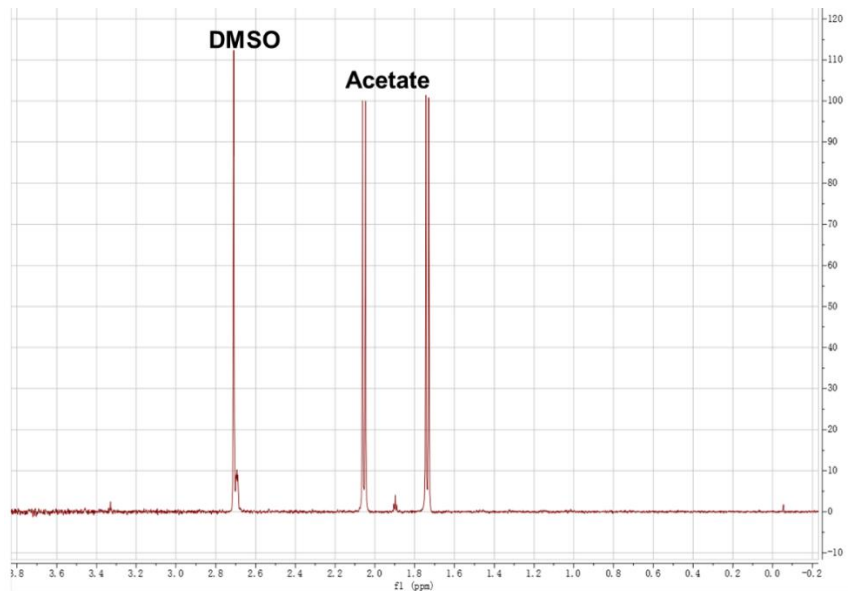
**Supplementary Fig. 21 | Schematic of pressurized flow cell system.**



**Supplementary Fig. 22 | NMR spectrum of liquid products from Cu/Ag-DA.** Representative  $^1\text{H}$ -NMR spectrum of catholyte with Cu/Ag-DA catalyst at  $-0.57 \text{ V}_{\text{RHE}}$  and 10 atm in 5 M KOH after 30 minutes of operation. DMSO is used as an internal standard. The peak near 3.33 ppm is assigned to methanol, the solvent used during catalyst deposition.

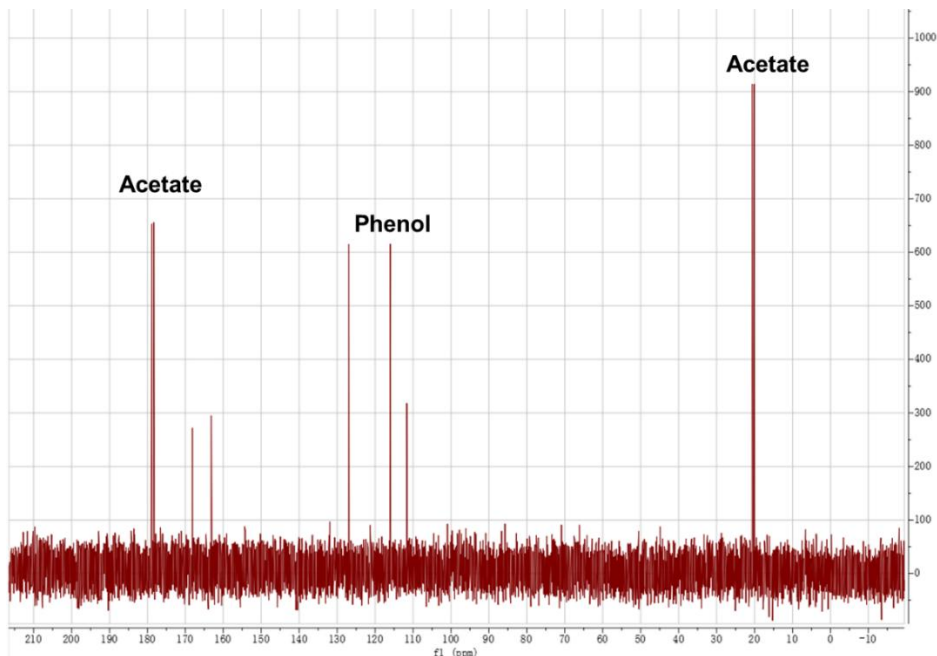


**Supplementary Fig. 23 | NMR spectrum of liquid products from Cu catalyst (Acetate, Ethanol, n-PrOH).** Representative  $^1\text{H}$ -NMR spectrum of catholyte with Cu catalyst at  $-0.57 \text{ V}_{\text{RHE}}$  and 1 atm in 5 M KOH after 40 minutes of operation. DMSO is used as an internal standard. The peak near 3.33 ppm is assigned to methanol, the solvent used during catalyst deposition.



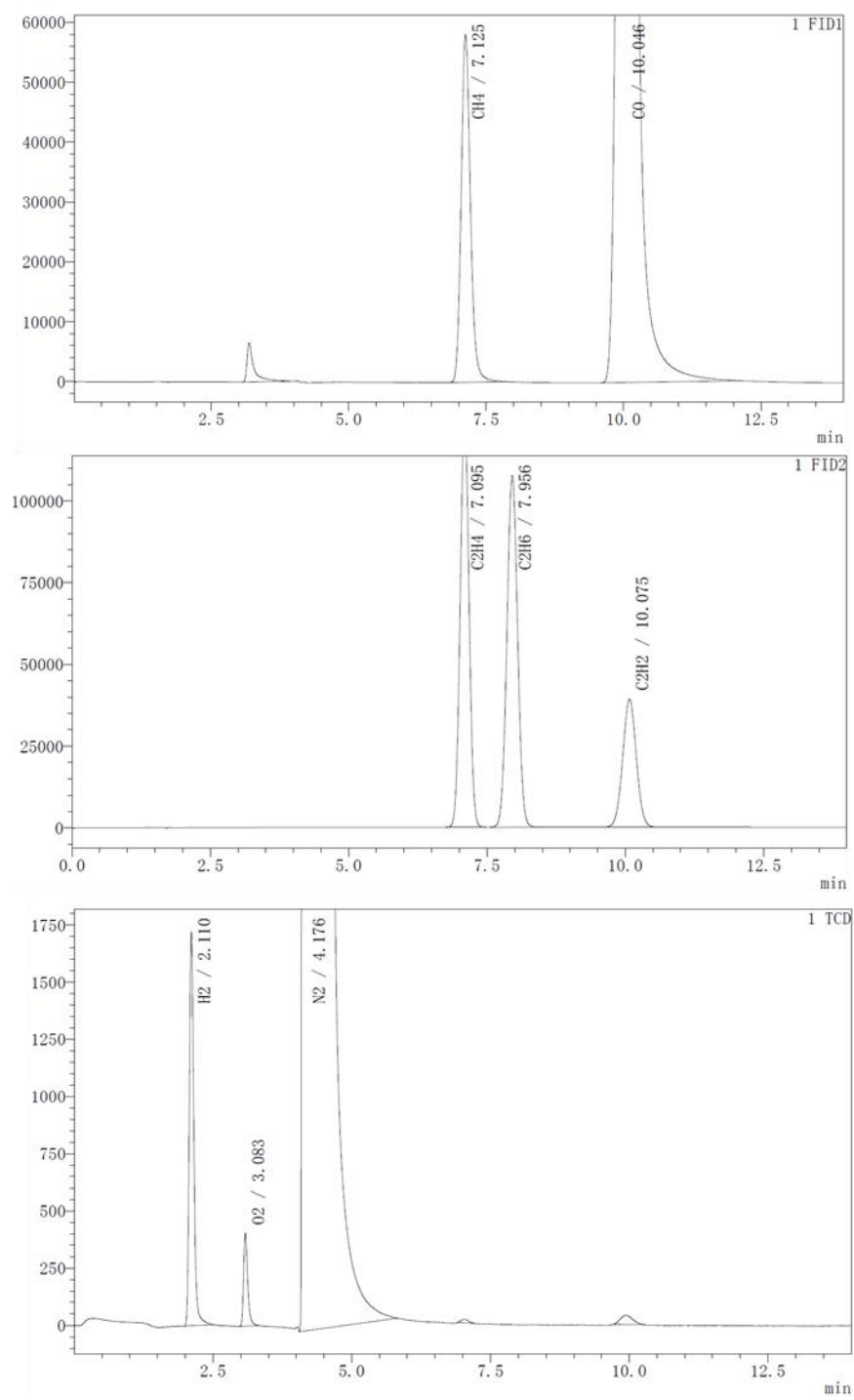
**Supplementary Fig. 24 | NMR spectrum of liquid products from Cu/Ag-DA using labeled C.**

Representative  $^1\text{H}$ -NMR spectrum of catholyte after  $^{13}\text{CORR}$  on Cu/Ag-DA GDE at -0.57 V vs. RHE in 5 M KOH. DMSO is used as an internal standard. The peak of acetate has split due to the effect of  $^{13}\text{C}$ <sup>22</sup>.

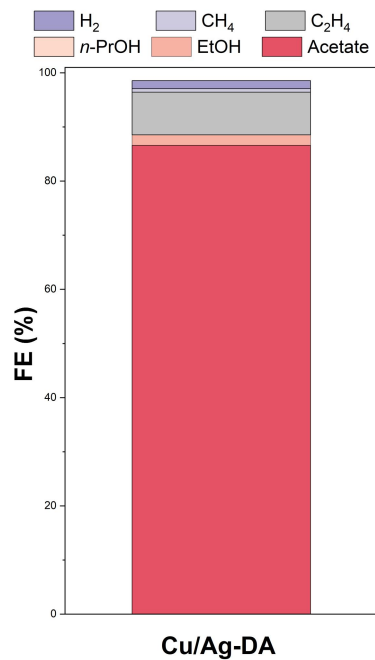


**Supplementary Fig. 25 | NMR spectrum of liquid products using Phenol as internal standard.**

Representative  $^{13}\text{C}$ -NMR spectrum of catholyte after  $^{13}\text{CORR}$  on Cu/Ag-DA GDE at -0.57 VRHE in 5 M KOH. Phenol is used as an internal standard. The peak of acetate has split due to the effect of  $^{13}\text{C}$ <sup>23</sup>, the peaks for acetate at 23.5 and 181.8 ppm, which correspond well with previously published data<sup>24</sup>.

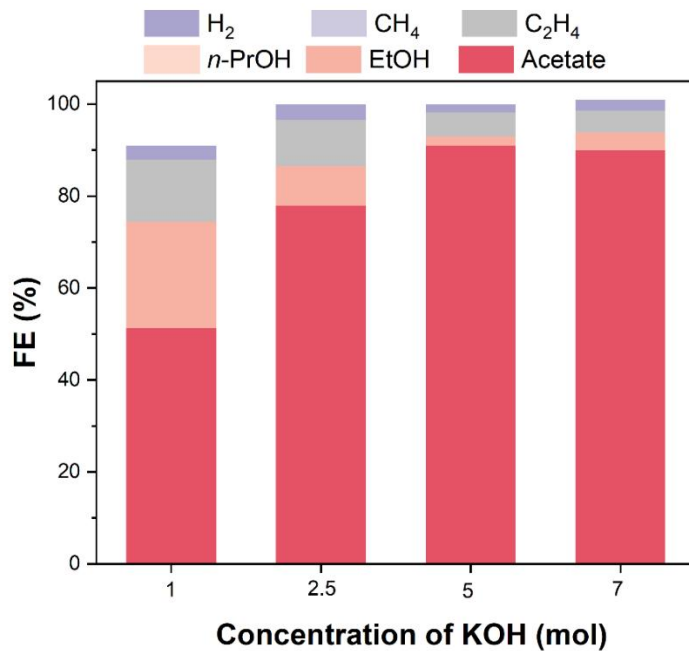


**Supplementary Fig. 26 | Gas chromatography analysis of the gas products of CORR.**

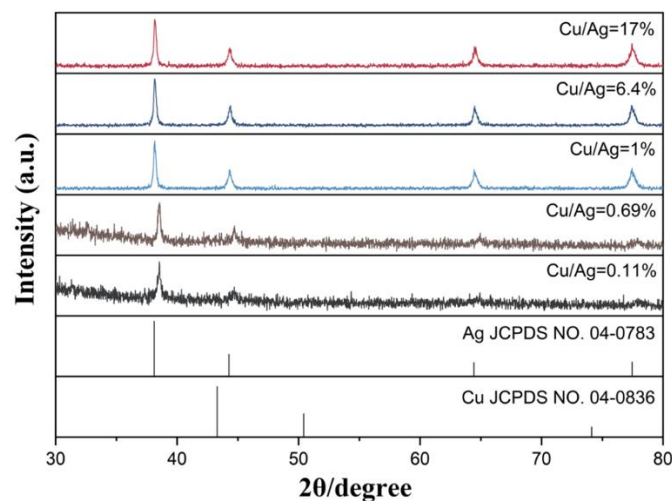


**Supplementary Fig. 27 | Low-flow CO electroreduction using Cu/Ag-DA.**

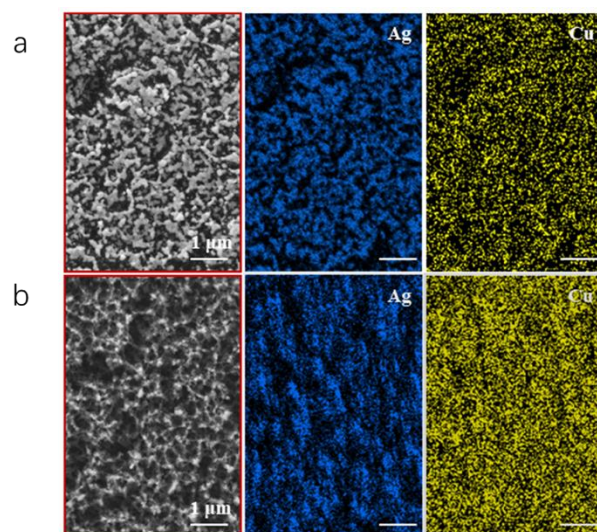
CO flow of 2 sccm and a potential of -0.7 V vs. RHE in 5 M KOH under 10 atm pressure.



**Supplementary Fig. 28 | CO electroreduction in a pressurized flow cell with varying concentration of KOH electrolyte.** Experimental data reported with a potential of -0.57 V vs RHE under 10 atm pressure.

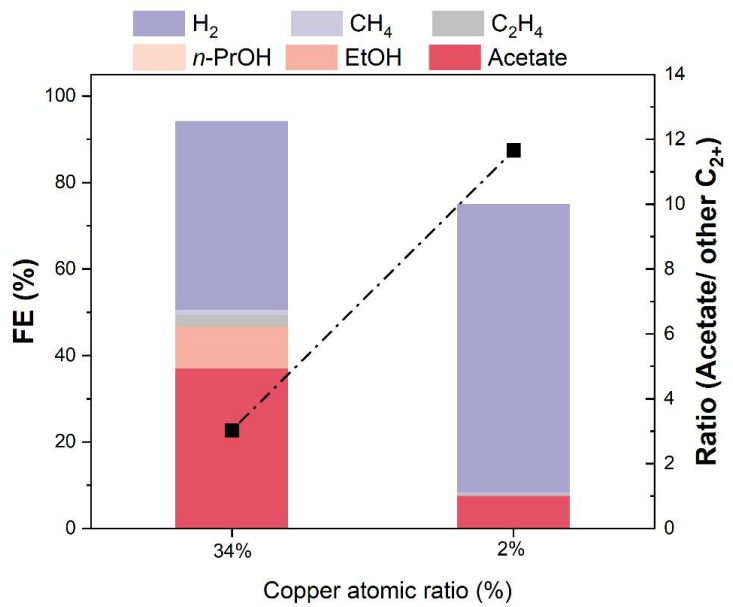


**Supplementary Fig. 29 | XRD patterns of the Cu/Ag-DA catalysts with varying relative atomic ratios of Cu to Ag.**

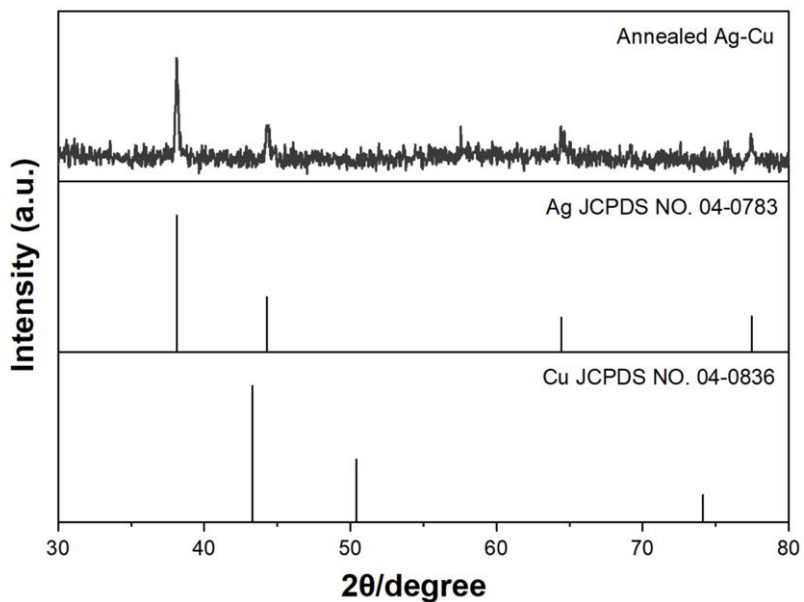


	Ag (at%)	O (at%)	Cu (at%)	R <sub>(Cu/Ag)</sub>
a	73.51	24.59	1.52	2%
b	35.61	45.14	18.72	34%

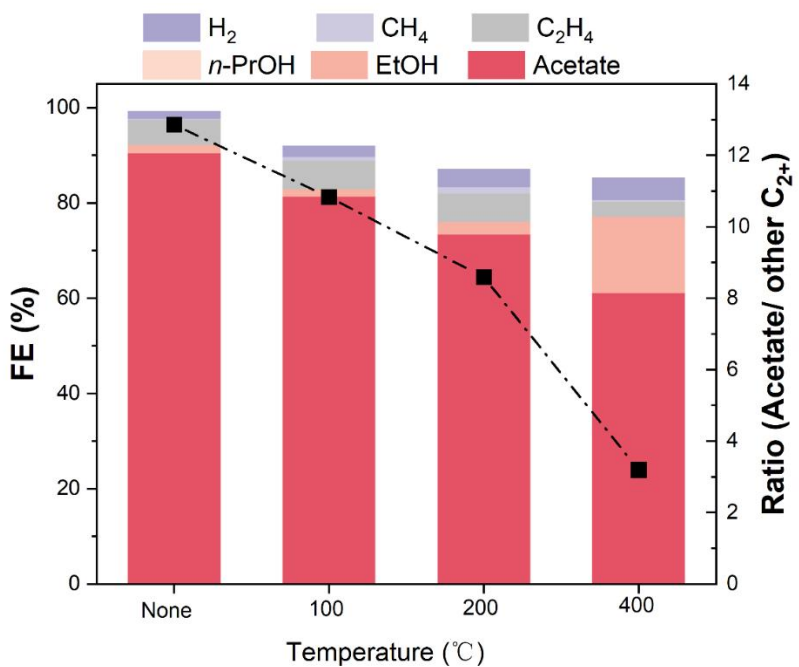
**Supplementary Fig. 30 | SEM and EDX mapping images of Cu/Ag-DA catalysts prepared with ion implantation.**



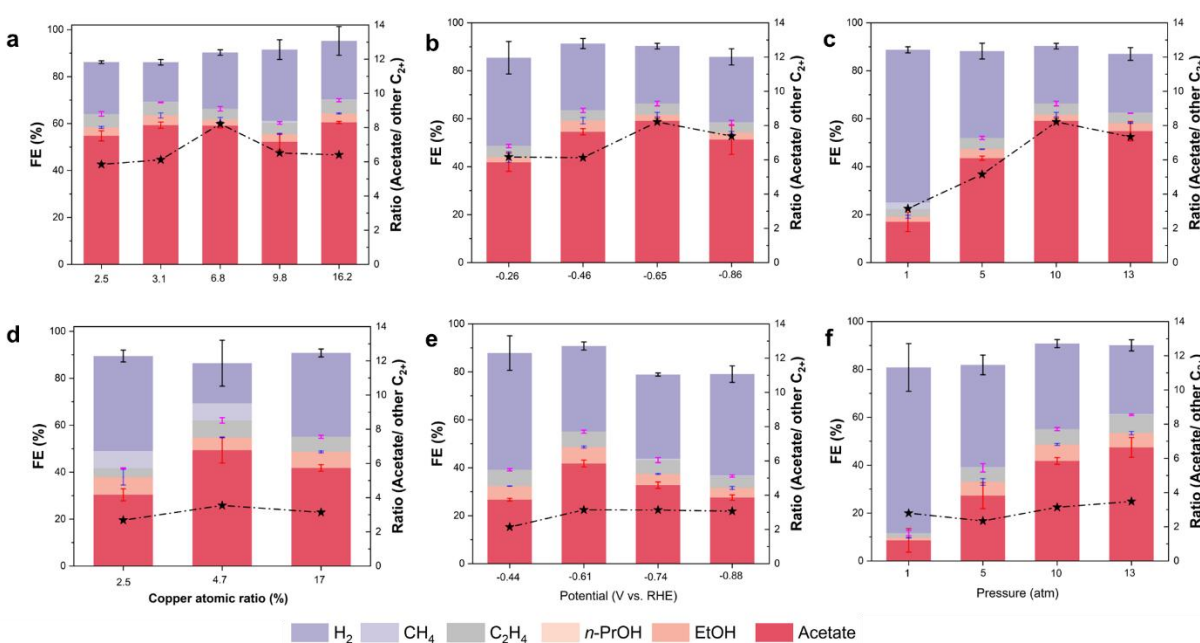
**Supplementary Fig. 31 | CO electroreduction performance of Cu/Ag-DA prepared by copper ion implantation.**



**Supplementary Fig. 32 | XRD of the Cu/Ag-DA catalysts with annealing temperature of 400°C**



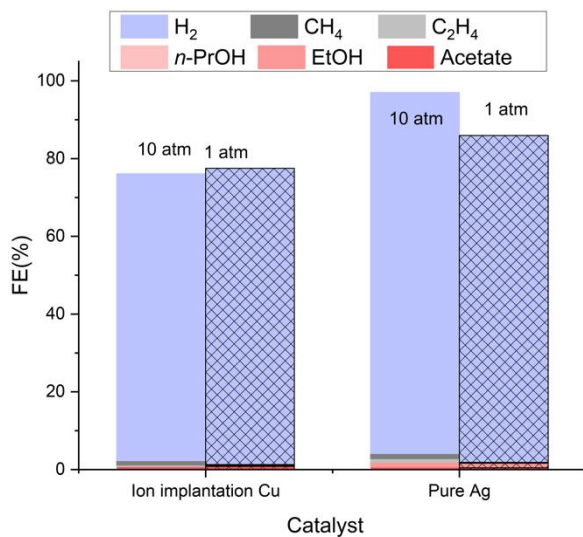
**Supplementary Fig. 33 | CO electroreduction performance of Cu/Ag-DA annealed at different temperatures** and measured at a potential of -0.57 V vs RHE in 5 M KOH under 10 atm pressure.



**Supplementary Fig. 34 | CO electroreduction in a pressurized flow cell with Cu/Au-DA (a-c) and Cu/Ni-DA (d-f) catalyst.** Unless otherwise specified, experimental data reported with a potential of -0.57 V vs RHE in 5 M KOH under 10 atm pressure. The Cu atomic ratios of Cu/Au-DA and Cu/Ni-DA catalysts in variable working conditions are 6.8% and 17%, respectively. (a, d) Effect of Copper atomic ratio; (b, e) Effect of applied potential; (c, f) Effect of CO partial pressure.

Experimental parameters for the control samples were varied in the order of Cu atomic ratio, applied potential, and pressure. For Cu/Au and Cu/Ni materials, the product distribution does not vary significantly when changing the Cu atomic ratio (unlike the Cu/Ag materials). Similarly, the applied potential for the composition carried through from a) to b) and d) to e) does little to change the ratio between acetate FE and the sum of FE from other  $C_{2+}$  products. We observe significant changes when pressure is modulated. For Cu/Au materials, Acetate FE is improved from ~16% to 60%. We also see a ~3x improvement in the ratio between acetate and other  $C_{2+}$  products as a result of increasing pressure from 1 atm to 13 atm. On the Cu/Ni surface, the absolute FE also improves, here to ~45%, but interestingly the ratio (acetate/ $C_{2+}$ ) does not change significantly. Therefore, improvement to FE on Cu/Ni surfaces is a result of  $H_2$  suppression and not necessarily a shift amongst carbon-based products.

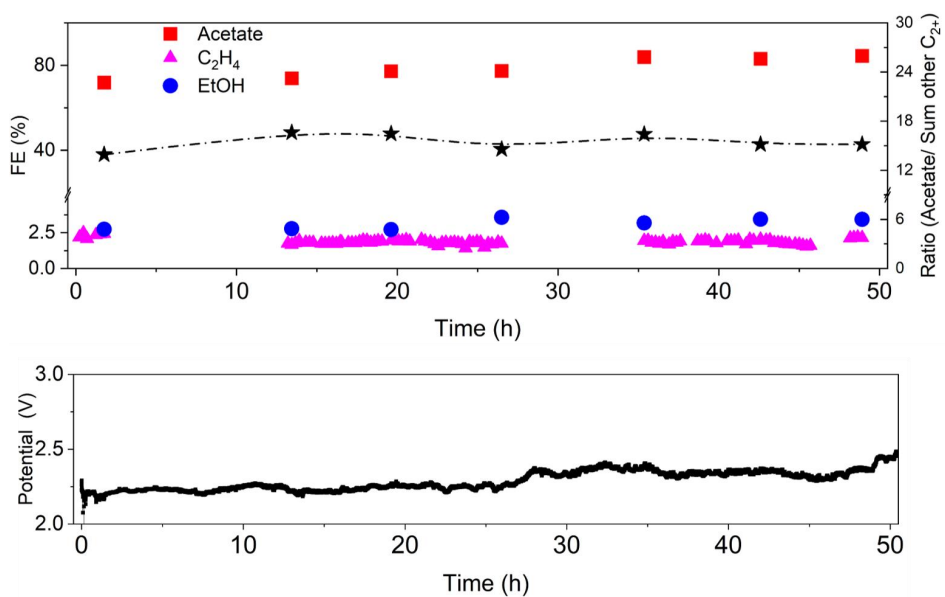
In instances where there is significantly more  $H_2$  production than with the Cu/Ag-DA materials, we found the total FE to be less than 100%. In the high-pressure electrolyzer, a fraction of  $H_2$  is dissolved in the cathode liquid and this fraction is not accounted for amongst the gaseous products measured at the cathode outlet and the liquid products measured at the anode outlet. This fraction of  $H_2$  was observed among the cathode liquid products via gas chromatography measurements.



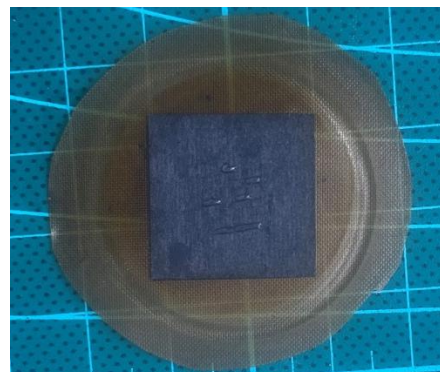
**Supplementary Fig. 35 | CO electroreduction in a pressurized flow cell using C and Ag control samples.** Cu/C-DA (prepared by ion implantation of Cu onto a carbon black substrate) and an Ag catalyst. Experimental data reported with a potential of -0.57V vs RHE in 5 M KOH.



**Supplementary Fig. 36 | Photograph of V1 MEA electrolyzer** with a  $1 \text{ cm}^2$  active geometric area of the flow field on each side.



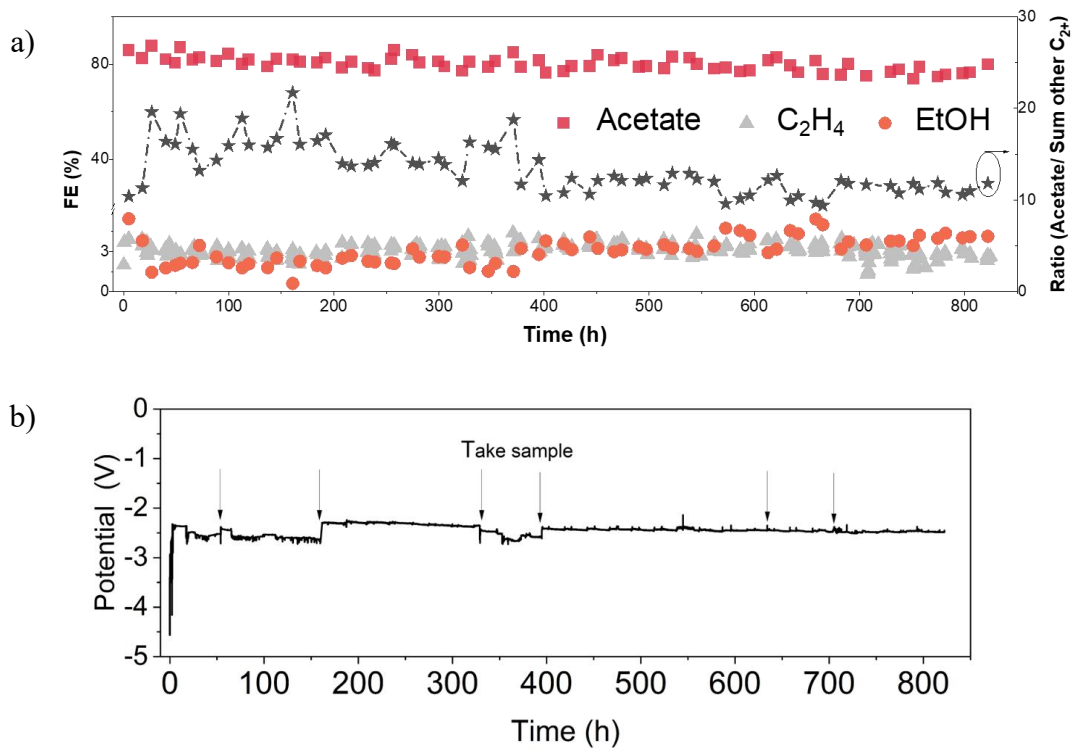
**Supplementary Fig. 37 | Stability demonstration of Cu/Ag-DA in the V1 MEA cell over 50 hours** at total current density of 100 mA/cm<sup>2</sup> in 5 M KOH at 20 atm. The concentration of acetate in the electrolyte is 1 M (1.7 mol%) at the completion of the 50-hour demonstration.



**Supplementary Fig. 38 | Image of liquid droplets on gas diffusion layer at the end of 50-hour experiment using the V1 pressurized MEA electrolyzer.**



**Supplementary Fig. 39 | Photograph of V2 MEA electrolyzer flow path** with 1 cm<sup>2</sup> active geometric area.



**Supplementary Fig. 40 | Stability demonstration of Cu/Ag-DA in the V2 MEA cell over >800 hours** at total current density of 100 mA/cm<sup>2</sup> in 2.5 M KOH at 10 atm. The sampling of liquid products led to voltage changes in some instances, notable changes are highlighted here. (a) Fig. 4e; (b) Voltage response over time. This experiment ended due to a pump failure.

### Supplementary Note: Stability Experiments

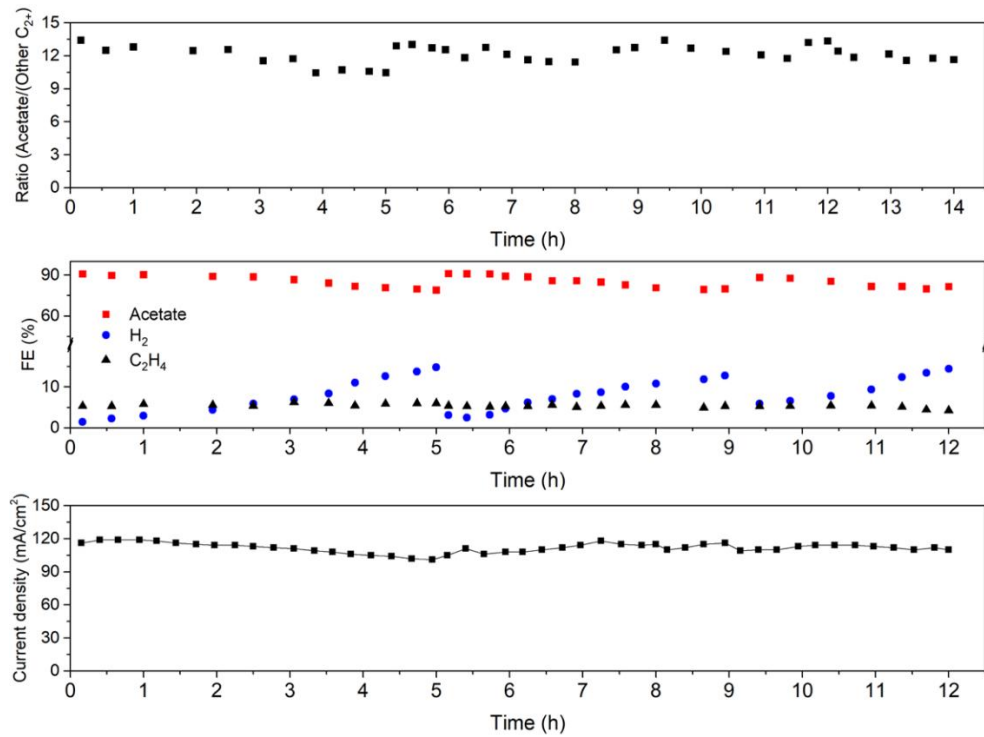
Notable improvements from the V1 MEA cell to the V2 MEA cell leading to improved stability:

1. Using a Sigracet 39BB gas diffusion layer instead of Freudenberg H14C9 (all other experiments in this work use Freudenberg H14C9, which we found to be stable on a 4-hour time-scale in the 10 atm flow cell and 50-hour time-scale in the 20 atm MEA)
  - Sigracet 39BB materials are 75% thicker (see Thickness), 5.5x stiffer (see Tensile Strength), and less porous (see Air Permeability).
  - These properties result in a substrate more resistant to flooding and more robust over time. By maintaining the position of the triple gas-solid-electrolyte boundary, we improved the stability of the reaction.

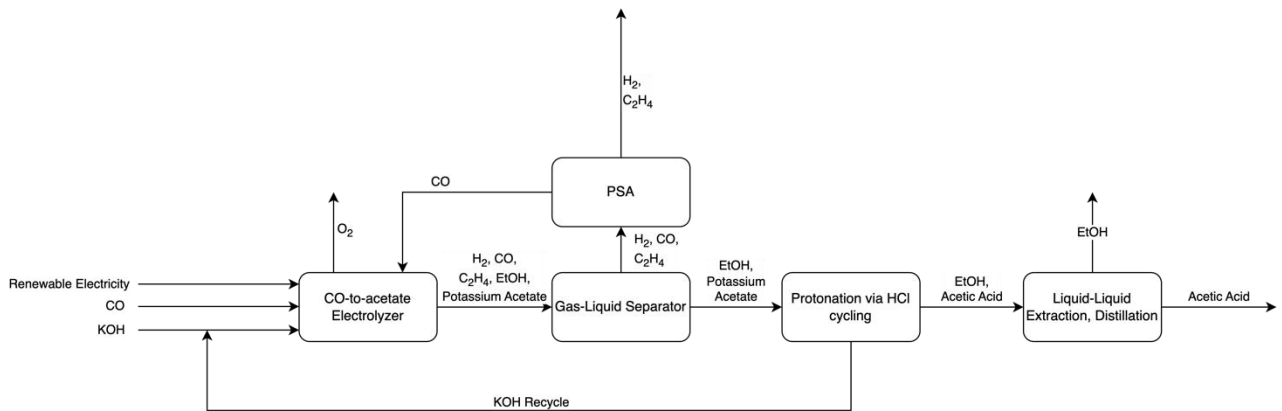
Name	Thickness	Area Weight	Tensile Strength	Through-Plane Air Permeability
Freudenberg C14H9	180 μm	100 g/m <sup>2</sup>	> 1.4 MPa	30 Gurley sec
Sigracet 39BB	315 μm	95 g/m <sup>2</sup>	7.7 MPa	1.5 Gurley sec

2. Re-engineering the gas flow channel of our MEA cell:
  - Using a more shallow flow channel (1 mm reduced to <0.2 mm)
  - Reducing the o-ring size around the flow channel (see [Supplementary Fig. 39](#))
3. Optimizing reaction conditions for improved stability by addressing two failure modes of our previous experimental lab set-up:

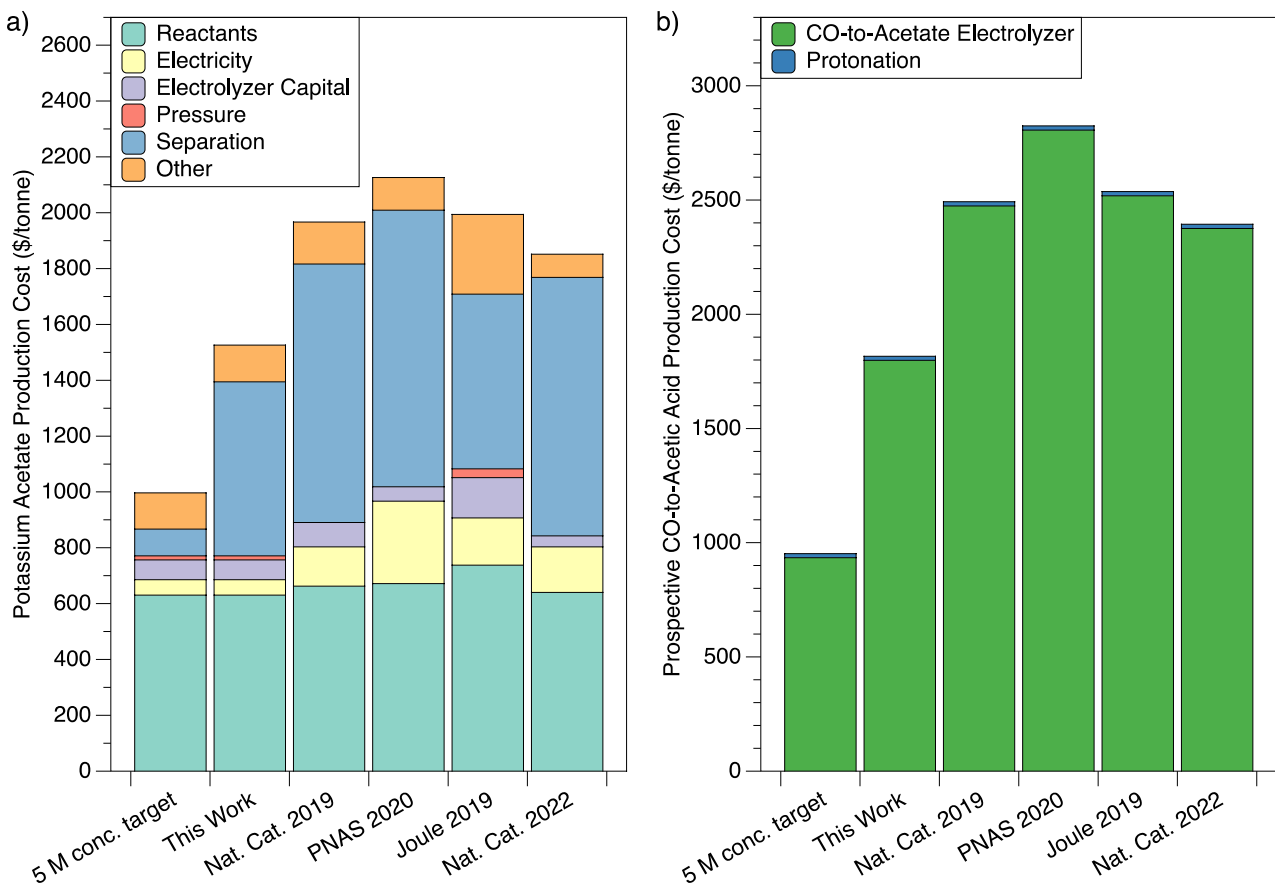
- Mitigating against pressure fluctuations in the system by reducing the flow rate of CO gas to 6.8 sccm and reducing the flow rate of electrolyte to 0.5 mL/min
- Mitigating against gas dissolved in the electrolyte leading to pump failure by continuously supplied fresh electrolyte to avoid the build-up of gas in the line



**Supplementary Fig. 41 | Stability test of CORR to acetate with Cu/Ag-DA in a flow cell during ~12 hours of electrolysis** at potential of -0.57 V vs RHE in 5 M KOH under 10 atm pressure. At the 5-hour and 9-hour timestamps, the catalyst was removed from the cell, rinsed, dried, and placed back into the cell with the same components. The recovery of performance is indicative of catalyst stability and the increase in H<sub>2</sub> is likely attributed to flooding of electrolyte into the gas diffusion layer.



**Supplementary Fig. 42 | Process flow of TRL=3 complexity to electro-synthesize acetic acid from CO.**



**Supplementary Fig. 43 | Techno-economic Analysis of (a) CO-to-potassium acetate and (b) CO-to-acetic acid compared with the best prior reports of acetate-O<sub>2</sub> electrolyzers.**

The *Reactants* component includes the costs for CO (carbon source), water (proton source) and KOH (potassium source) that result in Potassium Acetate. The *Electrolyzer Capital* component includes the electrolyzer capital costs, catalyst and membrane costs, as well as the cost of electrolyte (not including the electrolyte that is consumed into the product). The *Separation* component includes both operational and capital costs for gaseous and liquid separation. The *Other* component includes operational costs that do not fall into other categories (labor, miscellaneous supplies, etc), balance of plant and installation costs.

Data in the first column uses an identical set of performance metrics as this work, with the exception of a Potassium Acetate concentration of 5M instead of 1M. The concentration of acetate at the outlet of the reactor is a critical factor in reducing separation costs<sup>5</sup>. Higher concentrations have been reported using system-level advances in membrane design<sup>13</sup> and anodic oxidation reaction<sup>5</sup> selection. These approaches are compatible with the catalyst materials presented herein and would benefit cost reductions further by increasing product concentration.

## Supplementary Tables

**Supplementary Table 1 | Inductive coupled plasma optical emission spectroscopy (ICP-OES) of the as-synthesized Cu/Ag-DA catalysts.** The atomic % of Cu in Cu/Ag-DA catalysts is about 1%.

Sample	Cu (ppm)	Ag (ppm)	at. %Cu
Cu/Ag-DA-1	0.0676	10.8842	1.04
Cu/Ag-DA-2	0.0631	11.206	0.95

The formula for calculating the %Cu is as follows:

$$\% \text{Cu} = \frac{\text{Cu(ppm)}}{63.5} / \left( \frac{\text{Cu(ppm)}}{63.5} + \frac{\text{Ag(ppm)}}{107.9} \right)$$

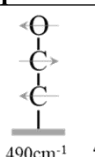
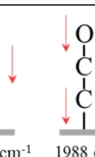
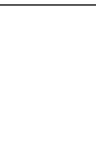
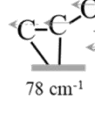
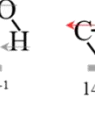
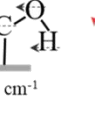
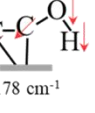
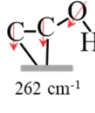
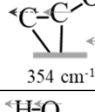
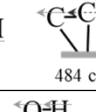
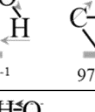
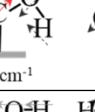
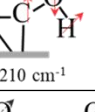
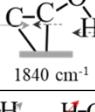
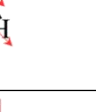
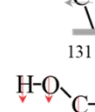
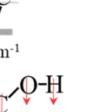
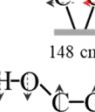
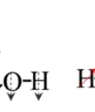
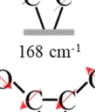
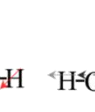
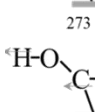
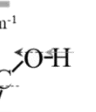
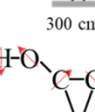
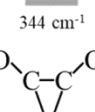
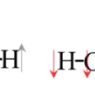
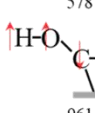
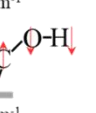
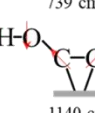
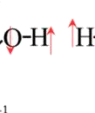
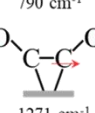
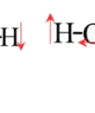
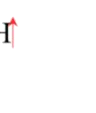
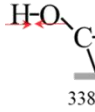
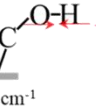
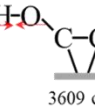
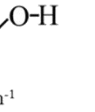
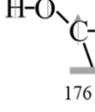
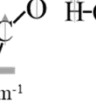
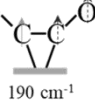
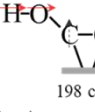
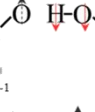
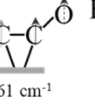
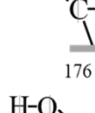
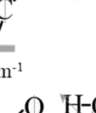
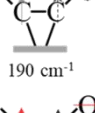
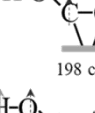
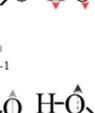
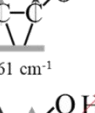
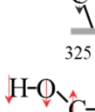
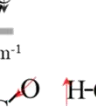
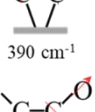
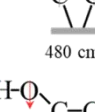
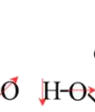
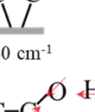
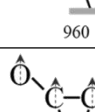
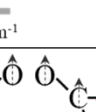
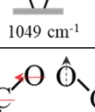
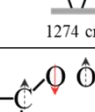
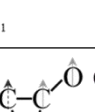
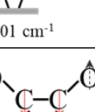
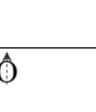
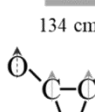
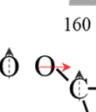
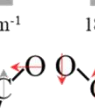
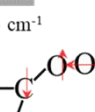
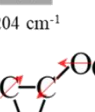
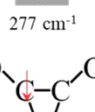
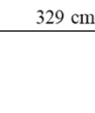
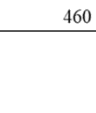
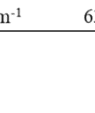
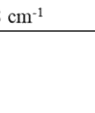
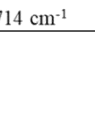
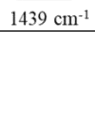
**Supplementary Table 2 | Cu atomic ratio of catalysts studied in this work**

Sample #	Catalyst type	Synthesis method	at. %Cu	Detection method
1	Cu/Ag-DA	Chemical synthesis	16.4	XPS
2	Cu/Ag-DA	Chemical synthesis	6.7	XPS
3	Cu/Ag-DA	Chemical synthesis	1	XPS, TEM-EDS, ICP-OES
4	Cu/Ag-DA	Chemical synthesis	0.7	SEM-EDS
5	Cu/Ag-DA	Chemical synthesis	0.8	SEM-EDS
6	Cu/Ag-DA	Chemical synthesis	0.1	SEM-EDS
7	Cu/Ag-DA	Ion implantation	2	SEM-EDS
8	Cu/Ag-DA	Ion implantation	34	SEM-EDS
9	Cu/Ni-DA	Chemical synthesis	2.5	XPS
10	Cu/Ni-DA	Chemical synthesis	4.7	SEM-EDS
11	Cu/Ni-DA	Chemical synthesis	17	SEM-EDS
12	Cu/Au-DA	Chemical synthesis	2.5	SEM-EDS
13	Cu/Au-DA	Chemical synthesis	3.1	SEM-EDS
14	Cu/Au-DA	Chemical synthesis	6.8	SEM-EDS
15	Cu/Au-DA	Chemical synthesis	9.8	SEM-EDS
16	Cu/Au-DA	Chemical synthesis	16.2	SEM-EDS

**Supplementary Table 3 | Cu K-edge EXAFS fitting results of Cu/Ag-DA during CORR at different potentials (vs. RHE).**

Cu/Ag-DA	Scatter path	Coordination number	Bond length (Å)	ΔE₀ (eV)	σ² (Å²)
-0.36 V	Cu-C	1.6	2.02	2.4	0.00531
	Cu-Cu	0.4	2.46	-5.3	0.00780
	Cu-Ag	6.2	2.78	-5.3	0.0137
-0.66 V	Cu-C	1.3	2.04	4.1	0.0109
	Cu-Cu	0.6	2.43	-1.8	0.0113
	Cu-Ag	5.9	2.65	-1.8	0.0123

**Supplementary Table 4 | Vibrational frequencies of C<sub>2</sub> species on Ag<sub>35</sub>Cu<sub>1</sub> with 1 layer of H<sub>2</sub>O.**  
The red, black, and grey arrows represent the plane, in-plane, out-of-plane vibrations.

	Vibrational frequencies								
*C=CO									
	108 cm <sup>-1</sup>	192 cm <sup>-1</sup>	205 cm <sup>-1</sup>	242 cm <sup>-1</sup>	308 cm <sup>-1</sup>	490 cm <sup>-1</sup>	543 cm <sup>-1</sup>	1210 cm <sup>-1</sup>	1988 cm <sup>-1</sup>
*C=COH									
	78 cm <sup>-1</sup>	119 cm <sup>-1</sup>	143 cm <sup>-1</sup>	178 cm <sup>-1</sup>	262 cm <sup>-1</sup>				
									
	354 cm <sup>-1</sup>	484 cm <sup>-1</sup>	972 cm <sup>-1</sup>	1210 cm <sup>-1</sup>	1840 cm <sup>-1</sup>				
*(HO)C=COH									
	131 cm <sup>-1</sup>	148 cm <sup>-1</sup>	168 cm <sup>-1</sup>	241 cm <sup>-1</sup>					
									
	273 cm <sup>-1</sup>	300 cm <sup>-1</sup>	344 cm <sup>-1</sup>	485 cm <sup>-1</sup>					
									
	578 cm <sup>-1</sup>	739 cm <sup>-1</sup>	790 cm <sup>-1</sup>	950 cm <sup>-1</sup>					
									
	961 cm <sup>-1</sup>	1140 cm <sup>-1</sup>	1271 cm <sup>-1</sup>	1447 cm <sup>-1</sup>					
									
	3384 cm <sup>-1</sup>	3609 cm <sup>-1</sup>							
*(HO)C=COH									
	176 cm <sup>-1</sup>	190 cm <sup>-1</sup>	198 cm <sup>-1</sup>	261 cm <sup>-1</sup>	278 cm <sup>-1</sup>				
									
	325 cm <sup>-1</sup>	390 cm <sup>-1</sup>	480 cm <sup>-1</sup>	640 cm <sup>-1</sup>	745 cm <sup>-1</sup>				
									
	960 cm <sup>-1</sup>	1049 cm <sup>-1</sup>	1274 cm <sup>-1</sup>	1401 cm <sup>-1</sup>	3491 cm <sup>-1</sup>				
*(O)C=CO									
	134 cm <sup>-1</sup>	160 cm <sup>-1</sup>	183 cm <sup>-1</sup>	204 cm <sup>-1</sup>	277 cm <sup>-1</sup>	298 cm <sup>-1</sup>			
									
	329 cm <sup>-1</sup>	460 cm <sup>-1</sup>	638 cm <sup>-1</sup>	714 cm <sup>-1</sup>	1439 cm <sup>-1</sup>	1558 cm <sup>-1</sup>			

**Supplementary Table 5 | Vibrational frequencies of C<sub>2</sub> species derived from <sup>12</sup>CO and <sup>13</sup>CO on Cu<sub>1</sub>Ag<sub>35</sub> model slab with 1 layer of H<sub>2</sub>O.**

Vibrational frequencies near the experimentally observed 541 cm<sup>-1</sup> peak are in red. The competing pathway \*C=COH does not have any vibrational frequencies within ±50 cm<sup>-1</sup> of this peak.

Adsorbate	Vibrational frequencies / cm <sup>-1</sup>															
	1988	1210	543	490	309	242	205	192	108							
* <sup>12</sup> C= <sup>12</sup> C=O	1919	1184	526	476	298	236	199	189	107							
* <sup>13</sup> C= <sup>13</sup> C=O	3334	1840	1210	972	485	354	326	262	179	143	119	78				
* <sup>12</sup> C= <sup>12</sup> COH	3334	1771	1207	954	483	343	316	253	175	141	117	76				
* <sup>13</sup> C= <sup>13</sup> COH	1558	1439	714	638	460	329	298	277	204	187	160	134				
*(O) <sup>12</sup> C= <sup>12</sup> CO	1406	1145	976	810	667	606	407	291	286	240	217	184				
*(O) <sup>13</sup> C= <sup>13</sup> CO	3491	1401	1274	1049	960	745	640	480	390	325	278	261	198	190	176	
*(O) <sup>12</sup> C= <sup>12</sup> COH	3487	1361	1265	1023	934	725	639	467	387	319	273	255	195	186	172	
*(HO) <sup>12</sup> C= <sup>12</sup> COH	3610	3384	1447	1271	1140	961	950	790	740	578	485	345	300	274	242	168
*(HO) <sup>13</sup> C= <sup>13</sup> COH	3609	3384	1404	1264	1132	934	928	790	724	576	472	342	294	271	239	146

**Supplementary Table 6 | Product FEs for Cu/Ag-DA under different applied potential in CORR.** Error bars represent the standard deviation of measurements based on three independent samples.

Potential (V vs Ag/AgCl)	Potential (V vs RHE)	Acetate (%)	EtOH (%)	n-PrOH (%)	C <sub>2</sub> H <sub>4</sub> (%)	CH <sub>4</sub> (%)	H <sub>2</sub> (%)	Total current density (mA/cm <sup>2</sup> )
-1.275	-0.23	32.6±3.2	0	0	15.1±0.2	0	26.1±0.1	1.6
-1.325	-0.28	70.0±0.7	0	0	7.0±0.8	0	15.2±1.9	4.2
-1.35	-0.30	75.5±2.4	0	0	6.1±0.2	0	14.6±0.2	8.2
-1.40	-0.34	81.4±1.0	0	0	5.6±0.2	0.2±0.1	7.2±0.7	14
-1.50	-0.43	82.5±2.4	0	0	6.0±0.4	0.2±0.1	9.1±0.5	33
-1.60	-0.51	86.7±1.2	3.7±0.5	0	3.7±0.5	1.7±0.2	2.1±0.5	60
-1.70	-0.57	91.2±1.6	1.8±0.1	0	5.2±0.1	0.2±0.1	1.7±0.3	123
-1.85	-0.68	89.6±1.1	1.5±0.2	0	6.9±0.6	0.1±0.1	1.9±0.1	170
-2.00	-0.79	83.6±2.5	3.2±0.3	0	4.1±0.3	0	2.7±0.4	234
-2.30	-0.99	73.7±5.5	2.0±0.5	0	5.2±0.8	0	9.7±1.5	355

**Supplementary Table 7 | Comparison of prior CO<sub>2</sub>/CO-to-acetate reports.**

Catalysts	Pressure	FE (%)	jacetate (mA/cm <sup>2</sup> )	EE acetate, full-cell (%)	Stability (FE ; time)	Reference
<b>Cu/Ag-DA</b>	<b>10 atm</b>	<b>85</b>	<b>85</b>	<b>34</b>	<b>85%; 820 h</b>	<b>This work (MEA)</b>
	<b>10 atm</b>	<b>81</b>	<b>11</b>	<b>34</b>	-	<b>This work (Flow-cell)</b>
		<b>91</b>	<b>113</b>	<b>27</b>	-	<b>This work (Flow-cell)</b>
		<b>84</b>	<b>196</b>	<b>16</b>	-	<b>This work (Flow-cell)</b>
	<b>1 atm</b>	<b>69</b>	<b>51</b>	<b>21</b>	-	<b>This work (Flow-cell)</b>
Cu–Pd pairs	1 atm	70	425	14 <sup>a</sup>	43%; 500 h	<i>Nat. Catal.</i> 5, 251–258 (2022). <sup>25</sup>
Mo oxide clusters modified Cu	1 atm	49	54	6	-	<i>Appl. Catal. B Environ.</i> 281, (2021). <sup>12</sup>
Triangular Cu nanosheets	1 atm	48	96	14 <sup>b</sup>	40%; 3 h	<i>Nat. Catal.</i> 2, 423–430 (2019). <sup>26</sup>
Cu nanotubes	1 atm	43	194	10	35%; 150 h	<i>Proc. Natl. Acad. Sci.</i> 118, (2021). <sup>13</sup>
Cu	4 atm	30	44	11	20%; 24 h	<i>Joule.</i> 3, 240–256 (2019). <sup>27</sup>

<sup>a</sup> This work did not report an anodic potential of the flow cell, we took the MEA cell data from the article to calculate the full cell energy efficiency (FE of acetate 50%; Potential 3.3V).

<sup>b</sup> This work did not report an anodic potential so we assume the same value as in our work.

**Supplementary Table 8 | Raw Data for Fig. 4a**

Product FEs for Cu/Ag-DA under different CO partial pressures in CORR. Error bars represent the standard deviation of measurements based on three or more independent samples.

CO partial pressure (atm)	Acetate (%)	EtOH (%)	<i>n</i> -PrOH (%)	C <sub>2</sub> H <sub>4</sub> (%)	CH <sub>4</sub> (%)	H <sub>2</sub> (%)
0.25	23.8±2.5	11.0±1.3	0	6.6±1.4	6.4±0.5	36.5±4.0
0.5	38.2±2.3	9.6±1.4	0	8.7±0.7	7.1±1.1	24.7±3.1
0.75	54.0±0.4	6.9±0.9	0	16.8±2.4	4.6±0.1	12.1±3.9
1	69.1±2.5	5.6±0.1	0	13.6±4.4	1.2±0.4	8.9±2.5
5	81.2±0.6	4.7±0.5	0	7.5±1.7	1.1±0.4	4.0±2.1
10	91.2±1.6	1.8±0.1	0	5.2±0.1	0.2±0.1	1.7±0.3
13	90.2±0.5	1.6±0.1	0	5.6±0.3	0.3±0.2	2.2±0.3

**Supplementary Table 9 | Raw Data for Fig. 4b**

Product FEs for Cu/Ag-DA under different applied potentials in CORR. Error bars represent the standard deviation of measurements based on three or more independent samples.

Potential (V vs RHE)	Acetate (%)	EtOH (%)	<i>n</i> -PrOH (%)	C <sub>2</sub> H <sub>4</sub> (%)	CH <sub>4</sub> (%)	H <sub>2</sub> (%)	Total Current Density (mA/cm <sup>2</sup> )
-0.28	70.0±0.7	0	0	7.0±0.8	0	15.2±1.9	4.2
-0.30	75.5±2.4	0	0	6.1±0.2	0	14.6±0.2	8.2
-0.34	81.4±1.0	0	0	5.6±0.2	0.2±0.1	7.2±0.7	14
-0.43	82.5±2.4	0	0	6.0±0.4	0.2±0.1	9.1±0.5	33
-0.51	86.7±1.2	3.7±0.5	0	3.7±0.5	1.7±0.2	2.1±0.5	60
-0.57	91.2±1.6	1.8±0.1	0	5.2±0.1	0.2±0.1	1.7±0.3	123
-0.68	89.6±1.1	1.5±0.2	0	6.9±0.6	0.1±0.1	1.9±0.1	170
-0.79	83.6±2.5	3.2±0.3	0	4.1±0.3	0	2.7±0.4	234
-0.99	73.7±5.5	2.0±0.5	0	5.2±0.8	0	9.7±1.5	355

**Supplementary Table 10 | Raw Data for Fig. 4c**

Product FEs for Cu/Ag-DA under different copper atomic ratio in CORR. Error bars represent the standard deviation of measurements based on three or more independent samples.

at. %Cu	Acetate (%)	EtOH (%)	<i>n</i> -PrOH (%)	C <sub>2</sub> H <sub>4</sub> (%)	CH <sub>4</sub> (%)	H <sub>2</sub> (%)
100	48.5±1.1	7.9±2.3	9.0±3.1	11.0±0.8	0	15.6±2.0
17.0	66.5±2.3	4.9±0.6	0	7.6±0.9	3.7±0.7	6.3±1.6
6.4	78.3±4.8	2.7±0.3	0	7.5±0.3	2.0±0.3	3.1±0.9
1.0	91.2±1.6	1.8±0.1	0	5.2±0.1	0.2±0.1	1.7±0.3
0.8	77.3±2.2	3.5±0.2	0	2.6±0.2	1.1±0.5	15.3±3.7
0.7	42.9±0.1	0.2±0.1	0	3.3±0.1	2.4±0.2	37.1±0.2
0.1	41.9±1.0	1.0±0.2	0	2.4±0.2	2.4±0.1	39.5±2.3
0	0.6±0.4	1.3±0.6	0	0.9±0.2	1.4±0.5	92.9±2.5

**Supplementary Table 11 | Raw Data for Fig. 4d**

Product FEs for Cu/M (Ag, Au, Ni)-DA under different copper atomic ratio in CORR.

Pressure (atm)	Catalyst	Acetate (%)	EtOH (%)	<i>n</i> -PrOH (%)	C <sub>2</sub> H <sub>4</sub> (%)	CH <sub>4</sub> (%)	H <sub>2</sub> (%)
1	Cu/Ag	69.1±2.5	5.6±0.1	0	13.6±4.4	1.2±0.4	8.9±2.5
	Cu/Au	17.0±4.0	2.2±0.6	0	3.2±0.1	2.8±1.2	63.7±1.3
	Cu/Ni	8.6±4.9	1.1±0.1	0	1.9±1.1	0	69.2±10.0
5	Cu/Ag	81.2±0.6	4.7±0.5	0	7.5±1.7	1.1±0.4	4.0±2.1
	Cu/Au	43.5±0.9	3.8±0.1	0	4.7±0.7	0	36.2±3.3
	Cu/Ni	27.3±5.4	5.7±1.4	0	5.9±1.8	0.3±0.1	42.7±4.1
10	Cu/Ag	91.2±1.6	1.8±0.1	0	5.2±0.1	0.2±0.1	1.7±0.3
	Cu/Au	59.1±1.0	2.6±0.9	0	4.7±1.0	0	24.0±1.2
	Cu/Ni	41.8±1.4	6.9±0.4	0	6.4±0.7	0	35.7±1.7
13	Cu/Ag	90.2±0.5	1.6±0.1	0	5.6±0.3	0.3±0.2	2.2±0.3
	Cu/Au	54.8±4.0	3.4±0.1	0	4.2±0.1	0.2±0.1	24.5±2.7
	Cu/Ni	47.4±4.1	6.0±0.7	0	7.7±0.3	0.3±0.1	28.7±2.3

**Supplementary Table 12 | Raw Data for Fig. 4e**

Catalyst stability in a MEA cell using Cu/Ag-DA at 10 atm at a current density of 100 mA/cm<sup>2</sup>.

Time (h)	Acetate/ (Other C <sub>2+</sub> )	Acetate (%)	EtOH (%)	C <sub>2</sub> H <sub>4</sub> (%)	H <sub>2</sub> (%)
5.0	10.4	85.8	5.5	2.8	15.1
17.9	11.3	82.4	3.8	3.5	13.0
26.8	19.6	87.6	1.5	3.0	13.7
40.1	16.4	82.0	1.8	3.2	12.8
49.2	16.1	80.4	2.0	3.0	13.5
54.0	19.4	87.0	2.1	2.4	15.0
65.6	15.6	82.0	2.2	3.1	11.8

72.2	13.2	82.8	3.5	2.8	12.6
88.3	14.4	81.3	2.6	3.1	12.6
99.9	15.9	84.4	2.2	3.1	13.2
112.8	18.9	79.9	1.8	2.5	12.7
119.2	16.0	81.8	2.1	3.0	12.9
137.1	15.8	78.9	1.8	3.2	12.5
145.7	16.7	82.2	2.5	2.4	13.3
160.8	21.7	81.9	0.6	3.2	13.6
167.8	16.1	81.0	2.3	2.8	14.4
184.2	16.5	80.6	2.0	2.9	16.1
192.2	17.1	82.6	1.8	3.0	14.8
208.0	14.0	78.5	2.5	3.1	14.6
216.7	13.7	80.9	2.7	3.2	13.9
232.5	13.8	77.2	2.2	3.4	15.5
238.8	14.1	78.4	2.3	3.3	13.6
254.6	16.1	82.1	2.2	2.9	19.1
257.4	16.0	85.8	2.1	3.3	19.6
274.9	14.1	83.9	3.2	2.8	12.6
281.4	13.9	80.6	2.6	3.2	19.1
299.6	14.5	81.1	2.6	3.0	11.6
305.3	13.9	79.0	2.6	3.1	16.0
322.3	12.1	77.1	3.5	2.9	12.7
329.2	16.3	80.9	1.8	3.2	11.6
346.9	15.8	78.8	1.5	3.5	14.6
353.7	15.5	81.3	2.1	3.1	12.3
370.9	18.7	84.9	1.5	3.0	12.0
378.1	11.7	78.8	3.2	3.5	16.1
395.0	14.4	81.6	2.8	2.9	12.7
401.7	10.5	76.3	3.8	3.5	12.9
418.6	10.8	76.9	3.6	3.5	12.3
426.2	12.4	79.1	3.2	3.2	11.2
443.3	10.6	79.1	4.1	3.3	10.8
451.0	12.1	83.8	3.2	3.7	14.1
466.5	12.6	81.5	3.0	3.5	10.8
473.7	12.2	82.4	3.1	3.7	14.9
490.4	12.1	78.7	3.4	3.1	12.6
497.1	12.3	79.2	3.2	3.2	15.6
514.2	11.7	78.2	3.5	3.2	13.2
522.0	12.9	83.1	3.3	3.2	15.0
538.2	12.9	82.6	3.2	3.2	10.2
545.4	12.3	80.0	3.0	3.5	12.3
561.7	12.0	78.1	3.4	3.1	13.5

572.7	9.6	78.6	4.8	3.4	16.3
586.4	10.1	76.8	4.6	3.0	13.0
595.6	10.5	77.3	4.2	3.1	11.2
613.0	12.2	81.6	2.9	3.8	15.7
621.3	12.7	82.8	3.2	3.4	13.8
634.2	10.0	79.3	4.6	3.4	11.6
641.7	10.4	76.5	4.3	3.0	13.1
658.4	9.7	81.3	5.4	2.9	12.1
665.1	9.4	75.7	5.0	3.0	11.5
682.4	12.1	75.5	3.2	3.0	11.7
689.4	11.8	80.0	3.7	3.0	11.2
706.4	11.7	75.0	3.5	2.9	13.0
729.5	11.5	76.7	3.8	2.8	13.9
737.5	10.7	77.8	3.8	3.4	18.7
751.0	11.8	73.8	3.5	2.8	20.5
757.0	11.2	78.8	4.2	2.8	20.1
774.4	11.9	74.7	4.0	2.3	19.5
781.9	10.8	75.6	4.4	2.6	20.0
798.0	10.6	76.0	4.0	3.1	20.1
805.0	11.0	76.5	4.1	2.8	21.1
822.0	11.8	79.9	4.1	2.6	19.8

**Supplementary Table 13 | Raw Data for Supplementary Fig. 28**

Product FEs for Cu/Ag-DA under different concentration of KOH electrolyte in CORR.

KOH Concentration (M)	Acetate (%)	EtOH (%)	n-PrOH (%)	C <sub>2</sub> H <sub>4</sub> (%)	CH <sub>4</sub> (%)	H <sub>2</sub> (%)
1	51.3	23.1	0	13.5	0	3.1
2.5	77.8	8.7	0	10.0	0	3.4
5	91.2	1.9	0	5.2	0	1.7
7	89.9	4.0	0	4.7	0	2.3

**Supplementary Table 14 | Raw Data for Supplementary Fig. 31**

CO electroreduction performance of Cu/Ag-DA prepared by copper ion implantation.

at. %Cu	Acetate (%)	EtOH (%)	n-PrOH (%)	C <sub>2</sub> H <sub>4</sub> (%)	CH <sub>4</sub> (%)	H <sub>2</sub> (%)
34	37.1	9.7	0	2.5	1.3	43.6
2.0	7.51	0	0	0.6	0.2	66.7

**Supplementary Table 15 | Raw Data for Supplementary Fig. 33**

CO electroreduction performance of Cu/Ag-DA annealed at different temperatures.

Temperature (°C)	Acetate (%)	EtOH (%)	n-PrOH (%)	C <sub>2</sub> H <sub>4</sub> (%)	CH <sub>4</sub> (%)	H <sub>2</sub> (%)
------------------	-------------	----------	------------	-----------------------------------	---------------------	--------------------

None	91.2	1.8	0	5.2	0.2	1.7
100	81.3	1.5	0	6.0	0.8	2.4
200	73.4	2.7	0	5.9	1.3	3.9
400	61.1	16.0	0	3.1	0.5	4.7

**Supplementary Table 16 | Raw Data for Supplementary Fig. 34a**

Product FEs for Cu/Au-DA under different copper atomic ratio in CORR.

at. %Cu	Acetate (%)	EtOH (%)	n-PrOH (%)	C <sub>2</sub> H <sub>4</sub> (%)	CH <sub>4</sub> (%)	H <sub>2</sub> (%)
2.5	54.8±2.2	3.6±0.4	0	5.8±1.0	0	22.0±0.6
3.1	59.3±1.3	4.1±1.1	0	5.6±0.2	0.2±0.1	16.9±1.2
6.8	59.1±1.0	2.6±0.9	0	4.6±1.0	0	24.0±1.2
9.8	52.3±3.5	3.3±0.2	0	4.7±0.6	0.9±0.1	30.4±4.2
16.2	60.5±0.5	3.8±0.2	0	5.6±0.6	0.5±0.3	24.9±6.1

**Supplementary Table 17 | Raw Data for Supplementary Fig. 34b**

Product FEs for Cu/Au-DA under different applied potentials in CORR.

Potential (V vs RHE)	Acetate (%)	EtOH (%)	n-PrOH (%)	C <sub>2</sub> H <sub>4</sub> (%)	CH <sub>4</sub> (%)	H <sub>2</sub> (%)
-0.26	41.8±3.8	2.2±2.1	0	4.6±0.7	0.05	36.8±6.8
-0.46	54.6±1.3	4.6±1.3	0	4.3±0.9	0.05	27.8±2.1
-0.65	59.1±1.0	2.6±0.9	0	4.6±1.0	0	24.0±1.2
-0.86	51.3±6.2	2.9±0.5	0	4.0±1.1	0.2±0.1	27.3±3.4

**Supplementary Table 18 | Raw Data for Supplementary Fig. 34c**

Product FEs for Cu/Au-DA under different CO partial pressures in CORR.

CO partial pressure (atm)	Acetate (%)	EtOH (%)	n-PrOH (%)	C <sub>2</sub> H <sub>4</sub> (%)	CH <sub>4</sub> (%)	H <sub>2</sub> (%)
1	17.0±4.0	2.2±0.6	0	3.2±0.1	2.8±1.2	63.7±1.3
5	43.5±0.9	3.8±0.1	0	4.7±0.7	0	36.2±3.3
10	59.1±1.0	2.6±0.9	0	4.7±1.0	0	24.0±1.2
13	54.8±4.0	3.4±0.1	0	4.2±0.1	0.2±0.1	24.5±2.7

**Supplementary Table 19 | Raw Data for Supplementary Fig. 34d**

Product FEs for Cu/Ni-DA under different copper atomic ratio in CORR.

at. %Cu	Acetate (%)	EtOH (%)	n-PrOH (%)	C <sub>2</sub> H <sub>4</sub> (%)	CH <sub>4</sub> (%)	H <sub>2</sub> (%)
2.5	30.4±2.6	7.5±3.4	0	3.8±0.1	7.3±7.1	40.5±2.5
4.7	49.4±5.5	5.4±0.1	0	7.3±1.2	7.3±1.2	17.1±9.8
17	41.8±1.4	6.9±0.4	0	6.4±0.7	0	35.7±1.7

**Supplementary Table 20 | Raw Data for Supplementary Fig. 34e**

Product FEs for Cu/Ni-DA under different applied potentials in CORR.

Potential (V vs RHE)	Acetate (%)	EtOH (%)	<i>n</i> -PrOH (%)	C <sub>2</sub> H <sub>4</sub> (%)	CH <sub>4</sub> (%)	H <sub>2</sub> (%)
-0.44	26.7±0.5	5.7±0.1	0	6.8±0.5	0	48.7±7.2
-0.61	41.8±1.4	6.9±0.4	0	6.4±0.7	0	35.7±1.7
-0.74	32.8±1.4	6.9±0.2	0	5.8±1.1	0.6±0.3	35.1±0.6
-0.88	27.6±1.1	4.0±0.6	0	4.9±0.4	0.3±0.1	42.3±3.4

**Supplementary Table 21 | Raw Data for Supplementary Fig. 34f**

Product FEs for Cu/Ni-DA under different CO partial pressures in CORR.

CO partial pressure (atm)	Acetate (%)	EtOH (%)	<i>n</i> -PrOH (%)	C <sub>2</sub> H <sub>4</sub> (%)	CH <sub>4</sub> (%)	H <sub>2</sub> (%)
1	8.6±4.9	1.1±0.1	0	1.9±1.1	0	69.2±10.0
5	27.3±5.4	5.7±1.4	0	5.9±1.8	0.3±0.1	42.7±4.1
10	41.8±1.4	6.9±0.4	0	6.4±0.7	0	35.7±1.7
13	47.4±4.1	6.0±0.7	0	7.7±0.3	0.3±0.1	28.7±2.3

**Supplementary Table 22 | Raw Data for Supplementary Fig. 37**

Catalyst stability in a MEA cell using Cu/Ag-DA at 20 atm.

Time (h)	Acetate/(Other C <sub>2+</sub> )	Acetate (%)	EtOH (%)	C <sub>2</sub> H <sub>4</sub> (%)	H <sub>2</sub> (%)	Potential (V)
1.8	13.9	71.9	2.7	2.4	14.3	2.21
13.3	16.6	73.9	2.8	1.7	15.5	2.20
19.4	16.5	77.2	2.7	2.0	13.5	2.26
26.5	14.6	77.3	3.6	1.7	11.7	2.26
35.0	16.4	83.9	3.2	1.9	12.4	2.36
42.4	15.2	83.1	3.4	2.0	11.3	2.35
49.6	15.2	84.4	3.4	2.1	12.5	2.44

**Supplementary Table 23 | Raw Data for Supplementary Fig. 41**

Catalyst stability in a flow cell using Cu/Ag-DA at 10 atm.

Time (h)	Acetate/(Other C <sub>2+</sub> )	Acetate (%)	C <sub>2</sub> H <sub>4</sub> (%)	H <sub>2</sub> (%)	Total current density (mA/cm <sup>2</sup> )
0.2	13.4	90.9	5.4	1.4	116
0.6	12.5	89.8	5.3	2.3	119
1.0	12.8	90.4	5.8	3.0	119
1.9	12.5	89.4	5.6	4.4	119
2.5	12.6	88.7	5.4	6.0	118
3.1	11.6	86.7	6.3	6.9	116
3.5	11.7	84.2	6.1	8.4	115

3.9	10.5	81.9	5.4	11.1	114
4.3	10.7	80.9	5.9	12.6	114
4.7	10.6	79.8	6.0	13.8	113
5.0	10.5	79.0	6.0	14.8	112
5.2	12.9	91.1	5.4	3.1	111
5.4	13.0	91.0	5.3	2.5	109
5.7	12.7	90.9	5.2	3.2	108
5.9	12.6	89.2	5.3	4.7	106
6.3	11.8	88.8	5.3	6.2	105
6.9	12.8	86.0	5.6	7.1	104
6.9	12.2	86.0	5.1	8.3	102
7.3	11.6	84.9	5.4	8.7	101
7.6	11.5	82.9	5.6	10.1	105
8.0	11.4	80.7	5.6	10.8	111
8.7	12.5	79.5	5.0	11.9	106
8.9	12.8	79.9	5.3	12.8	108
9.4	13.4	88.3	5.3	5.9	108
9.8	12.7	87.8	5.4	6.6	110
10.4	12.4	85.5	5.4	7.8	112
10.9	12.1	81.7	5.5	9.4	114
11.4	11.8	81.7	5.2	12.4	118
11.7	13.2	79.9	4.5	13.5	115
12.0	13.4	81.6	4.3	14.4	114

**Supplementary Table 24 | Techno-economic model parameters**

<b>Input Costs</b>	<b>Value</b>	<b>Reference</b>
CO (\$/tonne)	300.00	7
Water (\$/tonne)	5.00	7
Electricity (\$/kWh)	0.02	7
KOH (\$/tonne)	790.00	28
Electrolyte Concentration (M)	5	This work
Target Production of Potassium Acetate (tonne/day)	100	This work
<b>Reactor Performance</b>	<b>---</b>	
Acetate Faradaic Efficiency (%)	91	This work
Current Density (mA/cm <sup>2</sup> )	123 (flow cell); 100 (MEA cell)	This work
Cell Voltage (V)	3.1 (flow cell); 2.3 (MEA cell)	This work
Single-Pass Utilization (%)	70	This work
Product Concentration (%)	10	
<b>Plant Parameters</b>	<b>---</b>	
Reference Electrolyzer Cost (\$/kW)	450	2
Reference Current Density (mA/cm <sup>2</sup> )	400	2
Balance of Plant, BOP (%)	50	7,29
Lang Factor	1	7,29
Capacity Factor (%)	90	7,29
Electrolyzer Lifetime (years)	20	7,29
Catalyst + Membrane Lifetime (years)	5	7,29
Electrolyte Lifetime (years)	1	7,29
Discount Rate (%)	7	7,29
Maintenance Frequency (years <sup>-1</sup> )	5	7,29
Maintenance Factor (%)	10	7,29
Anolyte Volume (L/m <sup>2</sup> )	100	7,29
<b>Gas Separation</b>	<b>---</b>	
PSA Operational Cost (kWh/m <sup>3</sup> )	0.25	4
PSA Reference Capital Cost (\$)	1 989 043.00	4
PSA Reference Capacity (m <sup>3</sup> /h)	1000	4
PSA Capacity Scaling Factor	0.7	4
<b>Liquid Separation</b>	<b>---</b>	
Distillation Operational Cost (kWh/kg)	-326.9×ln(concentration[M]) + 620.95	5
Distillation Reference Capital Cost (\$)	4,162,240.00	4
Distillation Reference Capacity (m <sup>3</sup> /h)	1000	4
Distillation Capacity Scaling Factor	0.7	4

**Supplementary Table 25 | Raw Data for Supplementary Fig. 43**

Techno-Economic Analysis of CO-to-acetate.

	Reactants (\$/tonne)	Electricity (\$/tonne)	Electrolyzer Capital (\$/tonne)	Pressure (\$/tonne)	Separation (\$/tonne)	Other (\$/tonne)	Total (\$/tonne)
This work	630.36	55.21	70.87	14.87	623.00	131.66	1525.97
Ref. <sup>26</sup>	662.41	141.08	87.28	-	925.55	158.80	1966.53
Ref. <sup>13</sup>	671.48	295.64	51.57	-	990.62	124.84	2126.18
Ref. <sup>27</sup>	737.92	168.94	144.44	31.60	625.81	296.24	1993.82
Ref. <sup>25</sup>	640.27	162.68	39.75	-	925.70	83.22	1851.61

\* When acetate concentration was not provided, we assumed the same ratio between product and electrolyte concentration as in our work, i.e., 40 %, we achieve product concentration of 1 M with 2.5 M KOH

**Supplementary Table 26 | Free energy corrections.**

Species	E <sub>ZPE</sub> (eV)	$\int_0^{298} C_P dT$ (eV)	-TS (eV)	G-E (eV)
CO (g)	0.144	0.039	-0.610	-0.427
H <sub>2</sub> (g)	0.301	0.023	-0.404	-0.079
H <sub>2</sub> O (l)	0.567	0.050	-0.216	0.401
*CO	0.188	0.081	-0.121	0.148
*H	0.112	0.000	0.000	0.113
*C=C=O	0.330	0.058	-0.037	0.352
*C=COH	0.575	0.078	-0.243	0.410
*(OH)C=COH	1.014	0.134	-0.096	1.051
*OCCO	0.239	0.107	-0.085	0.261
*OCCOH	0.534	0.119	-0.095	0.559

**Supplementary Table 27 | Raw Data for Fig 1b, c.**

Cu <sub>1</sub> M <sub>35</sub> Surface	ΔG <sup>*</sup> (HO)C=COH → *C=C=O (eV)	ΔG <sup>*</sup> (HO)C=COH → *C=COH (eV)	ΔG <sup>*</sup> CO+CO → *OCCO (eV)	ΔG <sup>*</sup> OCCO → OCCOH (eV)
Cu <sub>1</sub> Ag <sub>35</sub>	-0.839	-0.092	-0.158	0.077
Cu <sub>1</sub> Au <sub>35</sub>	-0.510	0.265	0.331	0.024
Cu <sub>1</sub> Pd <sub>35</sub>	0.626	0.091	1.965	0.513
Cu <sub>1</sub> Pt <sub>35</sub>	0.622	0.193	1.518	0.008
Cu <sub>1</sub> Ni <sub>35</sub>	0.629	-0.353	2.356	-0.328

**Supplementary Table 28 | Raw Data for SI Fig 3.**

*CO Surface Coverage	ΔG <sub>CO</sub> (eV/Surface Atom) @ 1 atm	ΔG <sub>CO</sub> (eV/Surface Atom) @ 10 atm
1/9	-0.287	-0.293
2/9	-0.231	-0.244
3/9	-0.150	-0.169
4/9	-0.045	-0.071

**Supplementary Table 29 | Raw Data for Fig 1d. (Coverage Comparison)**

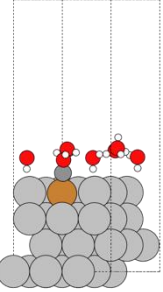
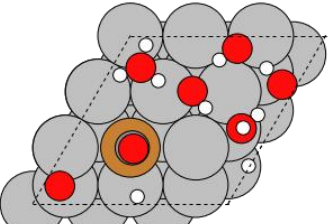
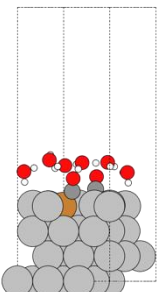
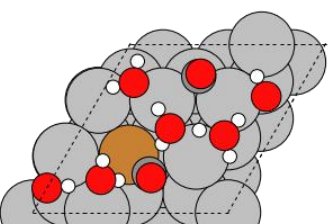
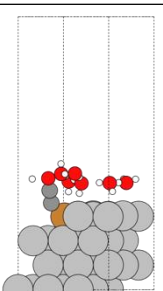
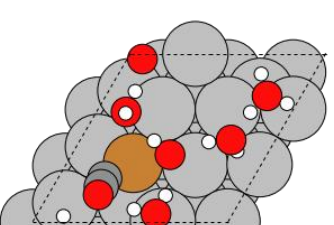
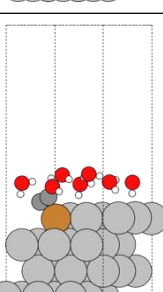
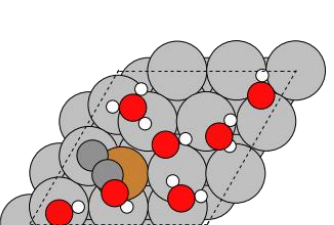
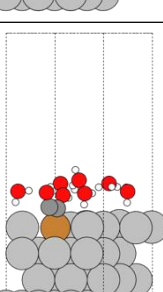
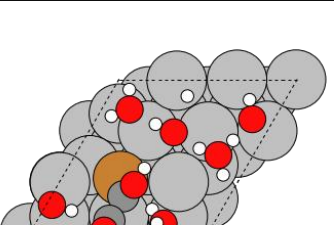
Coverage on Cu <sub>1</sub> Ag <sub>35</sub>	$\Delta G^*(\text{HO})\text{C}=\text{COH} \rightarrow * \text{C}=\text{C}=\text{O}$ (eV)	$\Delta G^*(\text{HO})\text{C}=\text{COH} \rightarrow * \text{C}=\text{COH}$ (eV)	$\Delta G^*(\text{HO})\text{C}=\text{COH} \rightarrow * \text{C}=\text{C}=\text{O} - \Delta G^*(\text{HO})\text{C}=\text{COH} \rightarrow * \text{C}=\text{COH}$ (eV)
2/9 ML	-0.839	-0.035	-0.804
3/9 ML	-1.152	0.239	-1.391
4/9 ML	-1.156	0.033	-1.189

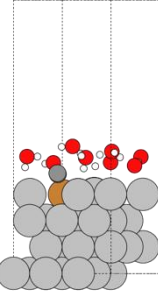
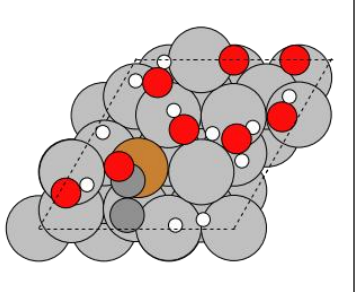
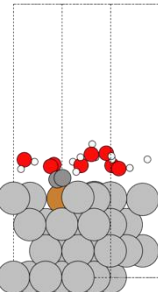
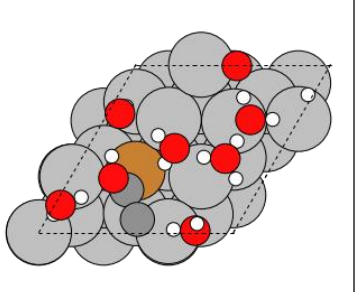
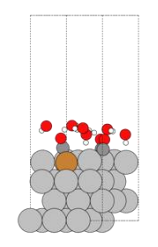
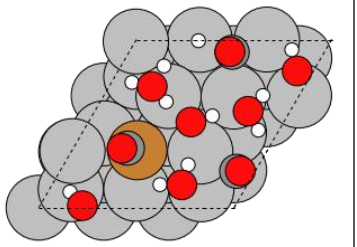
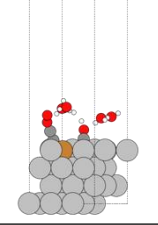
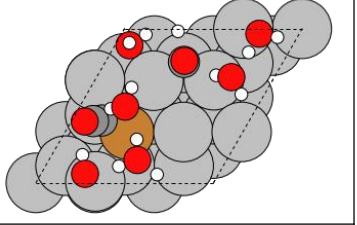
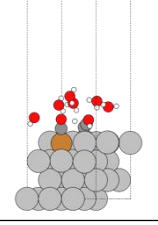
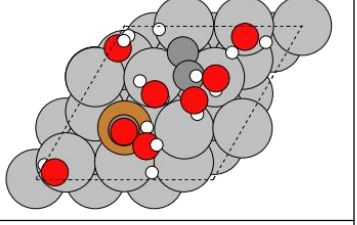
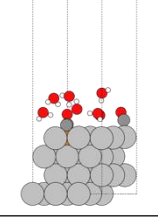
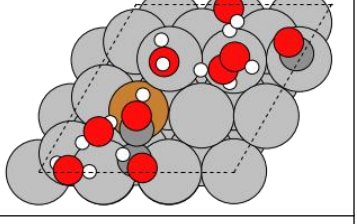
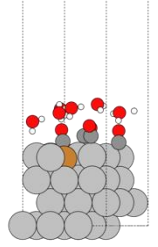
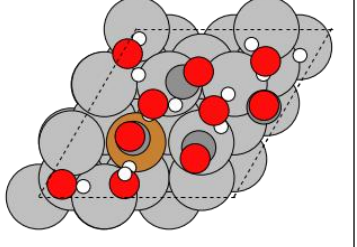
Coverage is defined by the number of carbon atoms among adsorbates per surface atoms in the unit cell in units ML (monolayer).

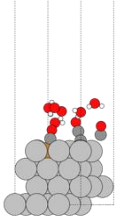
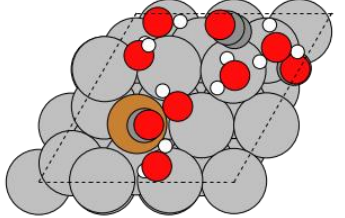
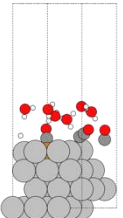
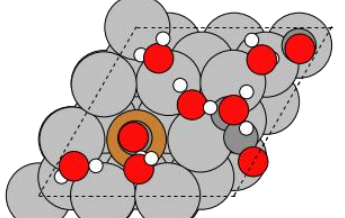
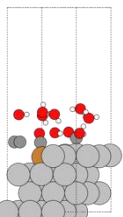
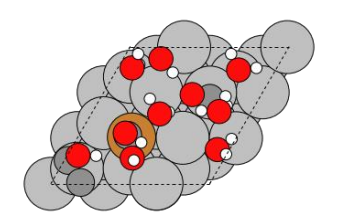
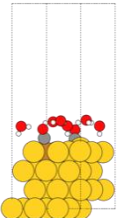
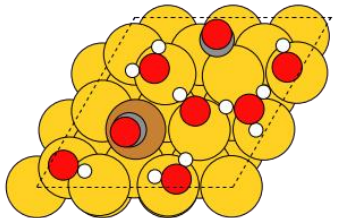
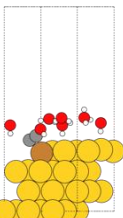
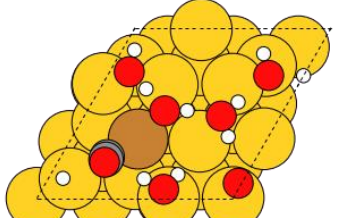
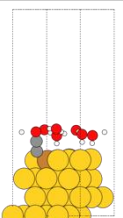
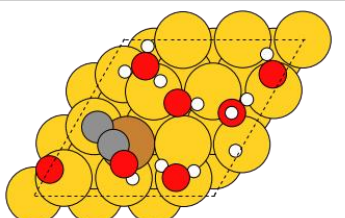
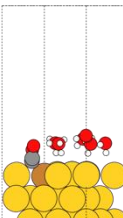
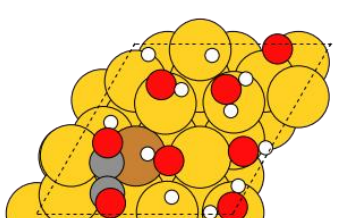
**Supplementary Table 30 | Raw Data for Fig 1d. (Cluster Comparison)**

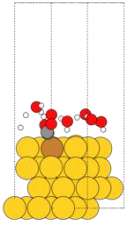
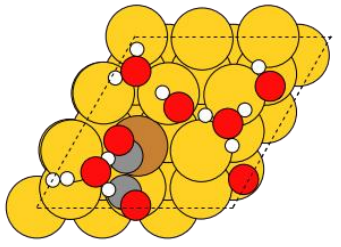
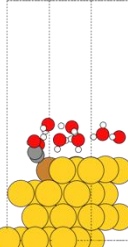
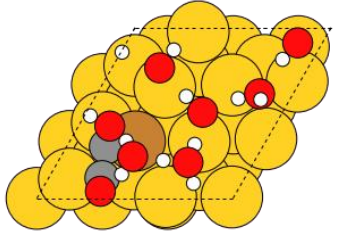
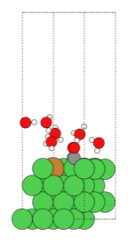
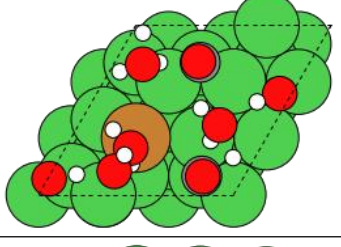
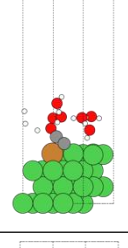
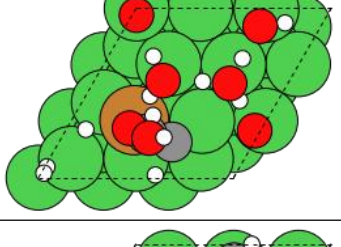
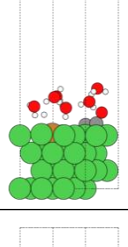
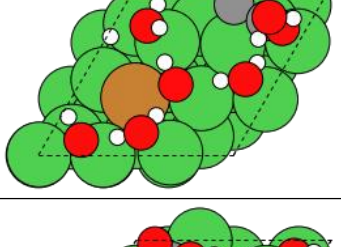
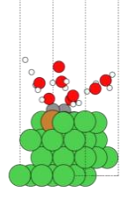
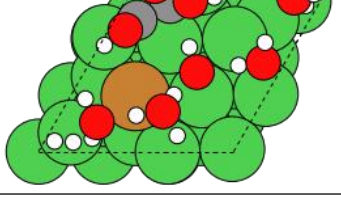
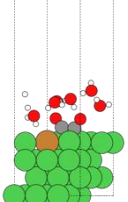
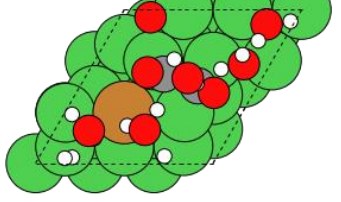
Surface	$\Delta G^*(\text{HO})\text{C}=\text{COH} \rightarrow * \text{C}=\text{C}=\text{O}$ (eV)	$\Delta G^*(\text{HO})\text{C}=\text{COH} \rightarrow * \text{C}=\text{COH}$ (eV)	$\Delta G^*(\text{HO})\text{C}=\text{COH} \rightarrow * \text{C}=\text{C}=\text{O} - \Delta G^*(\text{HO})\text{C}=\text{COH} \rightarrow * \text{C}=\text{COH}$ (eV)
Cu <sub>1</sub> Ag <sub>35</sub>	-0.839	-0.035	-0.804
Cu <sub>2</sub> Ag <sub>34</sub>	-0.883	-0.079	-0.804
Cu <sub>3</sub> Ag <sub>33</sub>	-1.071	-0.266	-0.805

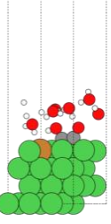
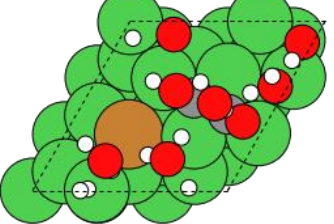
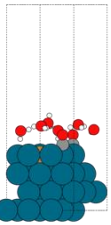
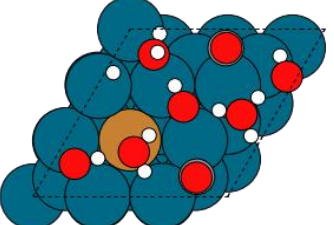
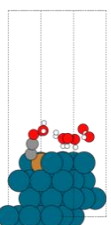
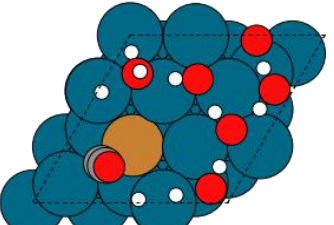
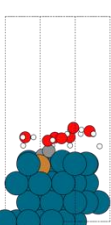
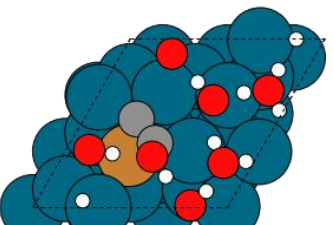
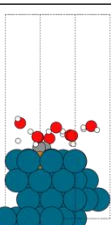
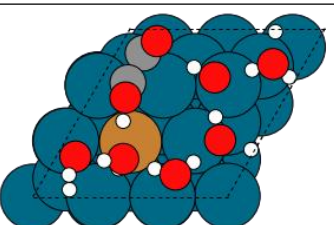
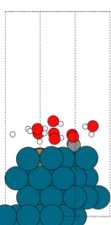
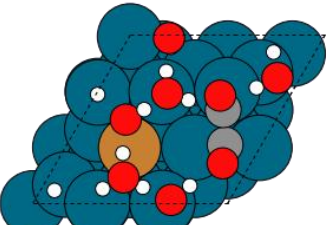
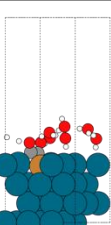
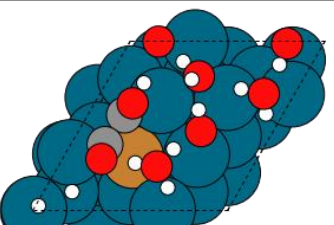
**Supplementary Table 31 | DFT Models (Source data provided).**

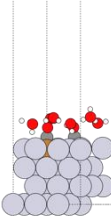
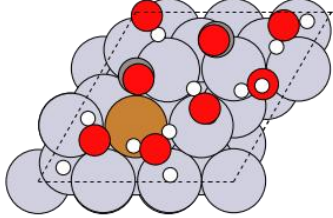
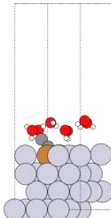
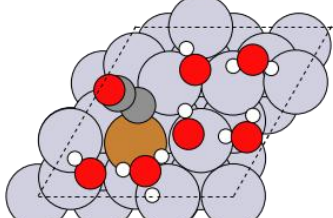
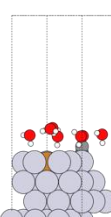
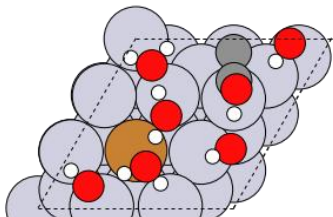
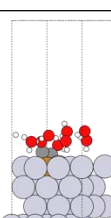
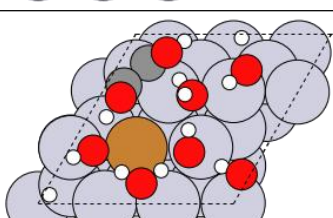
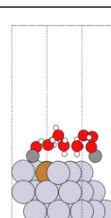
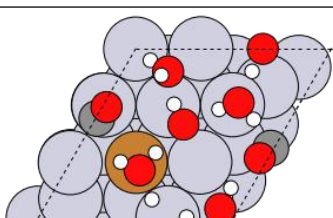
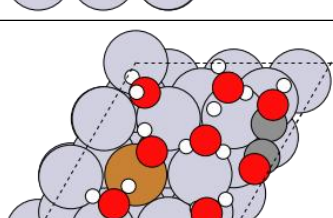
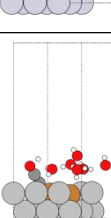
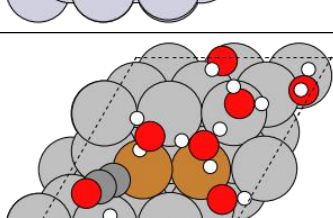
	Relevant Figure	Slab	Carbon coverage (ML)	Adsorbate	Total Energy (eV)	Side View	Top View
1	SI: 1	$\text{Cu}_1\text{Ag}_{35}$ (111)	1/9	*CO	-214.272		
2	1c, SI: 1	$\text{Cu}_1\text{Ag}_{35}$ (111)	2/9	*CO, *CO	-228.918		
3	1b, 1c, 1d	$\text{Cu}_1\text{Ag}_{35}$ (111)	2/9	*C=C=O	-222.524		
4	1b, 1c, 1d	$\text{Cu}_1\text{Ag}_{35}$ (111)	2/9	*C=COH	-225.050		
5	1b, 1c, 1d	$\text{Cu}_1\text{Ag}_{35}$ (111)	2/9	*(OH)C=COH	-236.213		

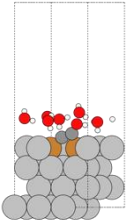
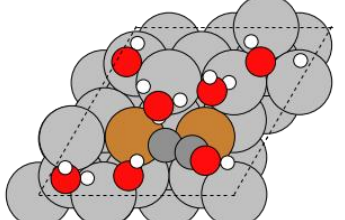
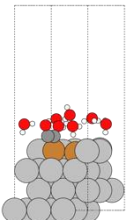
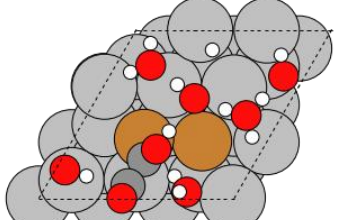
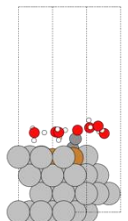
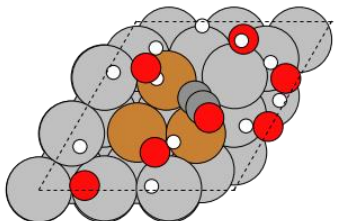
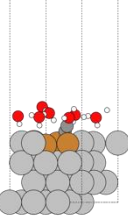
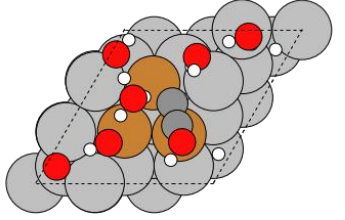
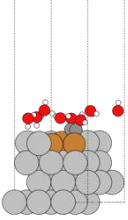
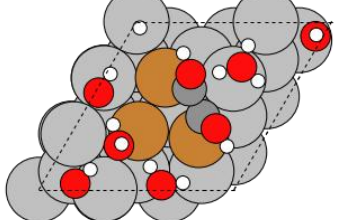
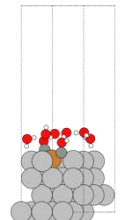
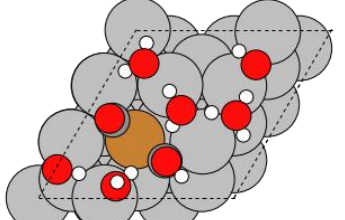
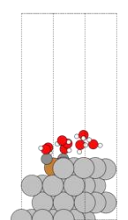
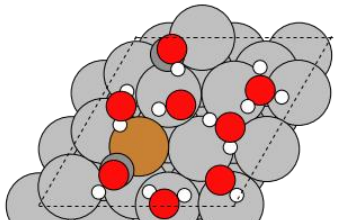
6	1c	$\text{Cu}_1\text{Ag}_{35}$ (111)	2/9	*CO-CO	-229.073		
7	1c	$\text{Cu}_1\text{Ag}_{35}$ (111)	2/9	*CO-COH	-232.588		
8	SI: 1	$\text{Cu}_1\text{Ag}_{35}$ (111)	3/9	*CO, *CO, *CO	-244.175		
9	1d	$\text{Cu}_1\text{Ag}_{35}$ (111)	3/9	*C=C=O, *CO	-237.101		
10	1d	$\text{Cu}_1\text{Ag}_{35}$ (111)	3/9	*C=COH, *CO	-239.378		
11	1d	$\text{Cu}_1\text{Ag}_{35}$ (111)	3/9	*(OH)C=COH, *CO	-250.815		
12	SI: 1	$\text{Cu}_1\text{Ag}_{35}$ (111)	4/9	*CO, *CO, *CO, *CO	-258.765		

13	1d	$\text{Cu}_1\text{Ag}_{35}$ (111)	4/9	*C=C=O, *CO, *CO	-252.539		
14	1d	$\text{Cu}_1\text{Ag}_{35}$ (111)	4/9	*C=COH, *CO, *CO	-254.679		
15	1d	$\text{Cu}_1\text{Ag}_{35}$ (111)	4/9	*(OH)C=COH, *CO, *CO	-265.910		
16	1b	$\text{Cu}_1\text{Au}_{35}$ (111)	2/9	*CO, *CO	-252.969		
17	1b, 1c	$\text{Cu}_1\text{Au}_{35}$ (111)	2/9	*C=C=O	-245.869		
18	1b, 1c	$\text{Cu}_1\text{Au}_{35}$ (111)	2/9	*C=COH	-248.365		
19	1b, 1c	$\text{Cu}_1\text{Au}_{35}$ (111)	2/9	*(OH)C=COH	-259.886		

20	1b, 1c	$\text{Cu}_1\text{Au}_{35}$ (111)	2/9	*CO-CO	-252.632		
21	1b, 1c	$\text{Cu}_1\text{Au}_{35}$ (111)	2/9	*CO-COH	-256.201		
22	1b	$\text{Cu}_1\text{Ni}_{35}$ (111)	2/9	*CO, *CO	-320.646		
23	1b, 1c	$\text{Cu}_1\text{Ni}_{35}$ (111)	2/9	*C=C=O	-310.645		
24	1b, 1c	$\text{Cu}_1\text{Ni}_{35}$ (111)	2/9	*C=COH	-314.898		
25	1b, 1c	$\text{Cu}_1\text{Ni}_{35}$ (111)	2/9	*(OH)C=COH	-325.800		
26	1b, 1c	$\text{Cu}_1\text{Ni}_{35}$ (111)	2/9	*CO-CO	-318.285		

27	1b, 1c	$\text{Cu}_1\text{Ni}_{35}$ (111)	2/9	*CO-COH	-322.206		
28	1b	$\text{Cu}_1\text{Pd}_{35}$ (111)	2/9	*CO, *CO	-319.442		
29	1b, 1c	$\text{Cu}_1\text{Pd}_{35}$ (111)	2/9	*C=C=O	-309.391		
30	1b, 1c	$\text{Cu}_1\text{Pd}_{35}$ (111)	2/9	*C=COH	-313.198		
31	1b, 1c	$\text{Cu}_1\text{Pd}_{35}$ (111)	2/9	*(OH)C=COH	-324.544		
32	1b, 1c	$\text{Cu}_1\text{Pd}_{35}$ (111)	2/9	*CO-CO	-317.471		
33	1b, 1c	$\text{Cu}_1\text{Pd}_{35}$ (111)	2/9	*CO-COH	-320.552		

34	1b	$\text{Cu}_1\text{Pt}_{35}$ (111)	2/9	*CO, *CO	-354.340		
35	1b, 1c	$\text{Cu}_1\text{Pt}_{35}$ (111)	2/9	*C=C=O	-345.272		
36	1b, 1c	$\text{Cu}_1\text{Pt}_{35}$ (111)	2/9	*C=COH	-348.973		
37	1b, 1c	$\text{Cu}_1\text{Pt}_{35}$ (111)	2/9	*(OH)C=COH	-360.421		
38	1b, 1c	$\text{Cu}_1\text{Pt}_{35}$ (111)	2/9	*CO-CO	-352.817		
39	1b, 1c	$\text{Cu}_1\text{Pt}_{35}$ (111)	2/9	*CO-COH	-356.403		
40	1d	$\text{Cu}_2\text{Ag}_{34}$ (111)	2/9	*C=C=O	-223.399		

41	1d	$\text{Cu}_2\text{Ag}_{34}$ (111)	2/9	*C=COH	-225.923		
42	1d	$\text{Cu}_2\text{Ag}_{34}$ (111)	2/9	<sup>*</sup> (OH)C=COH	-237.042		
43	1d	$\text{Cu}_3\text{Ag}_{33}$ (111)	2/9	*C=C=O	-224.488		
44	1d	$\text{Cu}_3\text{Ag}_{33}$ (111)	2/9	*C=COH	-227.012		
45	1d	$\text{Cu}_3\text{Ag}_{33}$ (111)	2/9	<sup>*</sup> (OH)C=COH	-237.943		
46	SI: 2	$\text{Cu}_1\text{Ag}_{35}$ (111)	2/9	*COH, *CO	-231.429		
47	SI: 2	$\text{Cu}_1\text{Ag}_{35}$ (111)	2/9	*COH, *COH	-233.447		

**Supplementary Note: Adsorption of C<sub>2</sub> intermediates on low Cu concentration surfaces**

Examining the C<sub>2</sub> adsorbates on Cu<sub>1</sub>Ag<sub>35</sub> surfaces (rows 3-7 in Supplementary Table 28 and the source data provided), we observe that for all bidentate C<sub>2</sub> adsorbates, one carbon adsorbs to the Cu atom or in a Cu-Ag bridge site, and the other carbon adsorbs to a Cu-Ag bridge site or a Cu-Ag-Ag hollow site. Based on this data, it does not appear that a single C<sub>2</sub> adsorbate is adsorbed entirely and only to the Cu atom. Ag alone is a traditionally weak binder of \*CO and multi-carbon adsorbates – hence the typical production of CO from CO<sub>2</sub> electroreduction on Ag catalysts. Pure Ag bind \*CO so weakly that it desorbs and does not permit further reduction. Here we use CO as a reactant, and we do not expect it to adsorb in regions of the catalyst that only have Ag. However, this assumption should not hold in the presence of Cu atom(s), which modulate the adsorption strength of nearby Ag atoms. With this in mind, Cu atoms and their neighboring Ag atoms are the regions of the catalyst where we expect electrocatalysis to proceed.

## References

1. Sisler, J. *et al.* Ethylene Electrosynthesis: A Comparative Techno-economic Analysis of Alkaline vs Membrane Electrode Assembly vs CO<sub>2</sub>-CO-C<sub>2</sub>H<sub>4</sub>Tandems. *ACS Energy Lett.* **6**, 997–1002 (2021).
2. Ruth, M.; Mayyas, A.; Mann, M. National Renewable Energy Laboratory. Manufacturing Competitiveness Analysis for PEM and Alkaline Water Electrolysis Systems. *Fuel Cell Semin. Energy Expo* (2017).
3. Hamelinck, C. N., Faaij, A. P. C., den Uil, H. & Boerrigter, H. Production of FT transportation fuels from biomass; technical options, process analysis and optimisation, and development potential. *Energy* **29**, 1743–1771 (2004).
4. Jouny, M., Luc, W. & Jiao, F. General Techno-Economic Analysis of CO<sub>2</sub> Electrolysis Systems. *Ind. Eng. Chem. Res.* **57**, 2165–2177 (2018).
5. Overa, S. *et al.* Enhancing acetate selectivity by coupling anodic oxidation to carbon monoxide electroreduction. *Nat. Catal.* **5**, 738–745 (2022).
6. Kibria, M. G. *et al.* Electrochemical CO<sub>2</sub> Reduction into Chemical Feedstocks: From Mechanistic Electrocatalysis Models to System Design. *Adv. Mater.* **1807166**, 1–24 (2019).
7. Ozden, A. *et al.* Cascade CO<sub>2</sub> electroreduction enables efficient carbonate-free production of ethylene. *Joule* **5**, 706–719 (2021).
8. Brynolf, S., Taljegard, M., Grahn, M. & Hansson, J. Electrofuels for the transport sector : A review of production costs. *Renew. Sustain. Energy Rev.* **81**, 1887–1905 (2018).
9. Huang, C., Xu, T., Zhang, Y., Xue, Y. & Chen, G. Application of electrodialysis to the production of organic acids: State-of-the-art and recent developments. *J. Memb. Sci.* **288**, 1–12 (2007).
10. Lopez, A. M. & Hestekin, J. A. Separation of organic acids from water using ionic liquid assisted electrodialysis. *Sep. Purif. Technol.* **116**, 162–169 (2013).
11. Alerte, T. *et al.* Downstream of the CO<sub>2</sub> Electrolyzer: Assessing the Energy Intensity of Product Separation. *ACS Energy Lett.* **6**, 4405–4412 (2021).
12. Zang, D. *et al.* Interface engineering of Mo<sub>8</sub>/Cu heterostructures toward highly selective electrochemical reduction of carbon dioxide into acetate. *Appl. Catal. B Environ.* **281**, 119426 (2021).
13. Zhu, P. *et al.* Direct and continuous generation of pure acetic acid solutions via electrocatalytic carbon monoxide reduction. *Proc. Natl. Acad. Sci. USA.* **118**, (2021).
14. Gao, J. *et al.* Selective C-C Coupling in Carbon Dioxide Electroreduction via Efficient Spillover of Intermediates As Supported by Operando Raman Spectroscopy. *J. Am. Chem. Soc.* **141**, 18704–18714 (2019).
15. Herzog, A. *et al.* Operando Investigation of Ag-Decorated Cu<sub>2</sub>O Nanocube Catalysts with Enhanced CO<sub>2</sub> Electroreduction toward Liquid Products. *Angew. Chemie - Int. Ed.* **60**, 7426–7435 (2021).
16. Moradzaman, M. & Mul, G. In Situ Raman Study of Potential-Dependent Surface Adsorbed Carbonate, CO, OH, and C Species on Cu Electrodes During Electrochemical Reduction of CO<sub>2</sub>. *ChemElectroChem* **8**, 1–9 (2021).
17. Ichiro Oda, Hirohito Ogasawara, and M. I. Carbon Monoxide Adsorption on Copper and Silver Electrodes during Carbon Dioxide Electroreduction Studied by Infrared Reflection Absorption Spectroscopy and Surface-Enhanced Raman Spectroscopy. *Langmuir* **12**, 1094–

- 1097 (1996).
- 18. Quilès, F. & Burneau, A. Infrared and Raman spectra of alkaline-earth and copper(II) acetates in aqueous solutions. *Vib. Spectrosc.* **16**, 105–117 (1998).
  - 19. Zhao, Y. *et al.* Speciation of Cu Surfaces during the Electrochemical CO Reduction Reaction. *J. Am. Chem. Soc.* **142**, 9735–9743 (2020).
  - 20. Cheng, T., Fortunelli, A. & Goddard, W. A. Reaction intermediates during operando electrocatalysis identified from full solvent quantum mechanics molecular dynamics. *Proc. Natl. Acad. Sci. USA.* **116**, 7718–7722 (2019).
  - 21. Itoh, T., Kajita, T., Maeda, T. & Kasuya, A. In situ surface-enhanced raman analysis of water librationon silver electrode in various alkali hydroxide aqueous solutions. *Electrochemistry* **82**, 396–400 (2014).
  - 22. Karapinar, D. *et al.* Electroreduction of CO<sub>2</sub> on Single-Site Copper-Nitrogen-Doped Carbon Material: Selective Formation of Ethanol and Reversible Restructuration of the Metal Sites. *Angew. Chemie - Int. Ed.* **58**, 15098–15103 (2019).
  - 23. Lum, Y. & Ager, J. W. Evidence for product-specific active sites on oxide-derived Cu catalysts for electrochemical CO<sub>2</sub> reduction. *Nat. Catal.* **2**, 86–93 (2019).
  - 24. Chatterjee, T., Boutin, E. & Robert, M. Manifesto for the routine use of NMR for the liquid product analysis of aqueous CO<sub>2</sub> reduction: From comprehensive chemical shift data to formaldehyde quantification in water. *Dalt. Trans.* **49**, 4257–4265 (2020).
  - 25. Ji, Y. *et al.* Selective CO-to-acetate electroreduction via intermediate adsorption tuning on ordered Cu–Pd sites. *Nat. Catal.* **5**, 251–258 (2022).
  - 26. Luc, W. *et al.* Two-dimensional copper nanosheets for electrochemical reduction of carbon monoxide to acetate. *Nat. Catal.* **2**, 423–430 (2019).
  - 27. Ripatti, D. S., Veltman, T. R. & Kanan, M. W. Carbon Monoxide Gas Diffusion Electrolysis that Produces Concentrated C<sub>2</sub> Products with High Single-Pass Conversion. *Joule* **3**, 240–256 (2019).
  - 28. Caustic Potash Price Trend and Forecast. <https://www.chemanalyst.com/Pricing-data/caustic-potash-1212>. 1–2 (2021).
  - 29. Wang, X. *et al.* Efficient electrosynthesis of *n*-propanol from carbon monoxide using a Ag–Ru–Cu catalyst. *Nat. Energy* **7**, 170–176 (2022).